

Reconstructing 1-km-resolution high-quality PM_{2.5} data records from 2000 to 2018 in China: spatiotemporal variations and policy implications

Jing Wei ^{a,b}, Zhanqing Li ^{b,*}, Alexei Lyapustin ^c, Lin Sun ^d, Yiran Peng ^e, Wenhao Xue ^a, Tianning Su ^b, Maureen Cribb ^b

^a State Key Laboratory of Remote Sensing Science, College of Global Change and Earth System Science, Beijing Normal University, Beijing, China

^b Department of Atmospheric and Oceanic Science, Earth System Science Interdisciplinary Center, University of Maryland, College Park, MD, USA

^c Laboratory for Atmospheres, NASA Goddard Space Flight Center, Greenbelt, MD, USA

^d College of Geodesy and Geomatics, Shandong University of Science and Technology, Qingdao, China

^e Ministry of Education Key Laboratory for Earth System Modeling, Department of Earth System Science, Tsinghua University, Beijing, China



ARTICLE INFO

Keywords:

PM_{2.5}
MODIS
Space-Time Extra-Trees model
ChinaHighPM_{2.5}
1 km resolution

ABSTRACT

Exposure to fine particulate matter (PM_{2.5}) can significantly harm human health and increase the risk of death. Satellite remote sensing allows for generating spatially continuous PM_{2.5} data, but current datasets have overall low accuracies with coarse spatial resolutions limited by data sources and models. Air pollution levels in China have experienced dramatic changes over the past couple of decades. However, country-wide ground-based PM_{2.5} records only date back to 2013. To reveal the spatiotemporal variations of PM_{2.5}, long-term and high-spatial-resolution aerosol optical depths, generated by the Moderate Resolution Imaging Spectroradiometer (MODIS) Multi-Angle implementation of Atmospheric Correction (MAIAC) algorithm, were employed to estimate PM_{2.5} concentrations at a 1 km resolution using our proposed Space-Time Extra-Trees (STET) model. Our model can capture well variations in PM_{2.5} concentrations at different spatiotemporal scales, with higher accuracies (i.e., cross-validation coefficient of determination, CV-R² = 0.86–0.90) and stronger predictive powers (i.e., R² = 0.80–0.82) than previously reported. The resulting PM_{2.5} dataset for China (i.e., ChinaHighPM_{2.5}) provides the longest record (i.e., 2000 to 2018) at a high spatial resolution of 1 km, enabling the study of PM_{2.5} variation patterns at different scales. In most places, PM_{2.5} concentrations showed increasing trends around 2007 and remained high until 2013, after which they declined substantially, thanks to a series of government actions combating air pollution in China. While nationwide PM_{2.5} concentrations have decreased by 0.89 µg/m³/yr ($p < 0.001$) during the last two decades, the reduction has accelerated to 4.08 µg/m³/yr ($p < 0.001$) over the last six years, indicating a significant improvement in air quality. Large improvements occurred in the Pearl and Yangtze River Deltas, while the most polluted region remained the North China Plain, especially in winter. The China-HighPM_{2.5} dataset will enable more insightful analyses regarding the causes and attribution of pollution over medium- or small-scale areas.

1. Introduction

In 2016, more than 92% of the world's population lived in areas experiencing pollution levels exceeding national acceptable limits. Air pollution has become one of the major environmental risks affecting human health and can raise the risk of death, respiratory diseases, and cardiovascular diseases (Brauer et al., 2012; Cohen et al., 2017; Liu et al., 2019a; Wei et al., 2019a, 2019b). About three million deaths per year are related to exposure to outdoor air pollution. In particular, fine

particulate matter (i.e., PM_{2.5}) has become the fifth leading lethal risk around the world. Long-term exposure to PM_{2.5} has resulted in 4.2 million deaths, accounting for 7.6% of deaths in 2015 globally and 59% of deaths in eastern and southern Asia, especially China (Beelen et al., 2014; Cohen et al., 2017; Song et al., 2019; Sun et al., 2016). PM_{2.5} pollution has thus become a great concern to the public.

Since the start of the twentieth century, the Chinese government has implemented a large number of policies to both promote the national economy and improve air quality. The Five-Year Plan (FYP) was

* Corresponding author.

E-mail addresses: weijing_rs@163.com (J. Wei), zli@atmos.umd.edu (Z. Li).

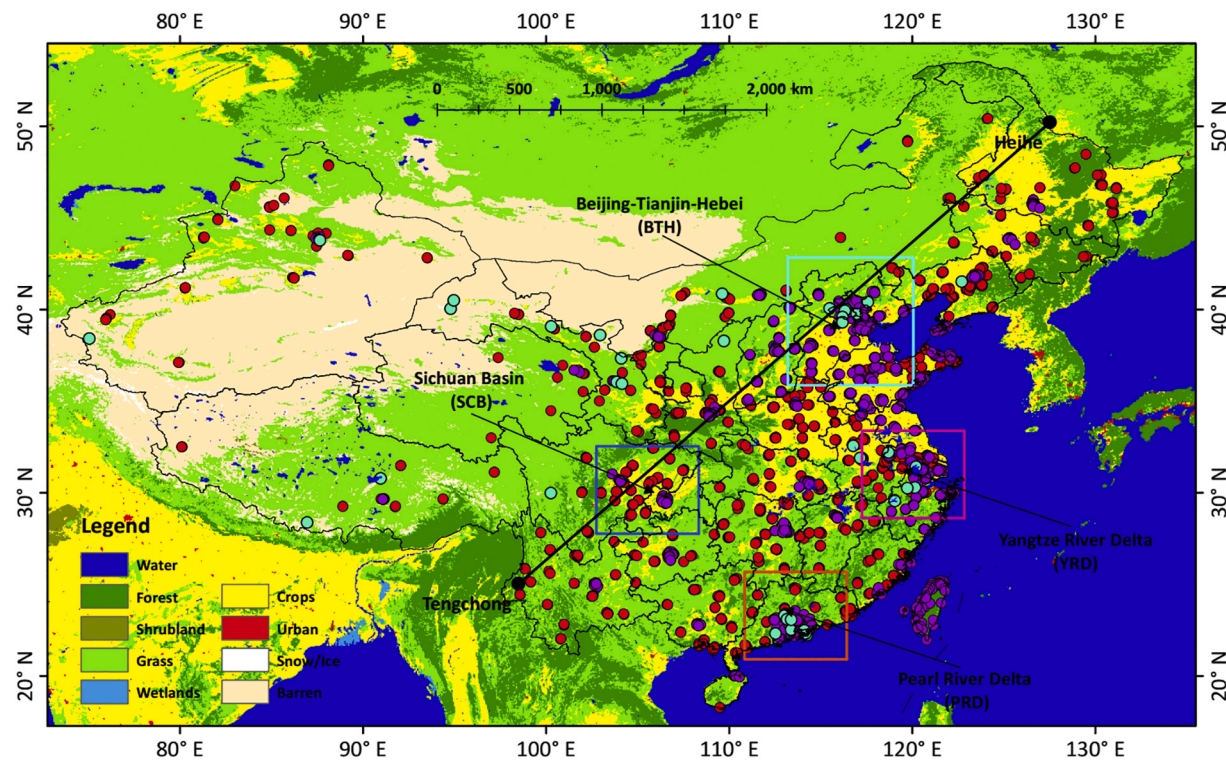


Fig. 1. Spatial distribution of ground PM_{2.5} monitoring stations in 2013 (purple dots) and newly established monitoring stations in 2018 (red dots), and AERONET AOD monitoring stations (green dots) across China. Background colors indicate the surface type. (For interpretation of the references to colour in this figure legend, the reader is referred to the web version of this article.)

designed for economic and social development and has been implemented every five years since 1953 in China. The latest FYPs include the 10th FYP (2001–2005), the 11th FYP (2006–2010), the 12th FYP (2011–2015), and the current (13th) FYP (2016–2020). In 2008, Beijing strengthened its environmental management and protection to prepare for the Olympic Games (Du and Mendelsohn, 2011; Shen et al., 2011), after which China continuously maintained regional air pollution control measures (Yana et al., 2016). In 2013, the national government had implemented the five-year Action Plan on Air Pollution Prevention and Control with the aim to significantly reduce PM_{2.5} pollution from 2013 to 2017 in China, especially in key urban agglomerations (Zhang et al., 2019a). In 2018, the national government rolled out a three-year Blue-Sky Defense (2018–2020) action plan to significantly reduce total major air pollutant emissions, with the aim to enhance the quality of life for the general public.

Over the years, remote sensing technology has been widely applied in estimating spatially continuous near-surface PM_{2.5} concentrations. Aerosol optical depth (AOD) products generated from multi-source satellites, e.g., the Moderate-resolution Imaging Spectroradiometer (MODIS; Ma et al., 2014; Wei et al., 2019, 2020), the Visible infrared Imaging Radiometer (VIIRS; Yao et al., 2019), and Himawari-8 (Zhang et al., 2019c; Su et al., 2020), have been employed as the most critical independent variable to derive PM_{2.5} concentrations due to their strongly positive relationships (Guo et al., 2009; van Donkelaar et al., 2006). Traditional physical methods have been used to derive daily PM_{2.5} concentrations by calculating the fine-mode fraction and correcting for humidity and altitude, but these PM_{2.5} estimates were poorly correlated with surface measurements (Yan et al., 2017; Zhang and Li, 2015). Statistical regression methods, e.g., the linear mixed-effect method (LME; Ma et al., 2014) and geographically weighted regression (GWR; Yu et al., 2017), were selected to improve daily PM_{2.5} estimates, achieving increased cross-validation coefficient of determination (CV-R²) values. Subsequently, machine or deep-learning methods, e.g., random forest, extreme gradient boosting, and deep belief network

models, were applied to obtain even more accurate daily PM_{2.5} estimates with CV-R² values greater than 0.8 (Chen et al., 2018; Chen et al., 2019; Li et al., 2017b; Wei et al., 2019a).

PM_{2.5} is jointly affected by both natural and human conditions, leading to complicated varying relationships with AOD, along with space and time changes. Traditional physical models cannot identify and explain PM_{2.5}-AOD relationships well. Statistical regression models have difficulty building stable PM_{2.5}-AOD relationships due to their weak data-mining abilities, resulting in poor accuracies of PM_{2.5} estimates. Machine/deep-learning approaches can mine useful information from a large amount of input data, but they are always directly applied, usually ignoring the essential characteristics of the spatiotemporal heterogeneity, as well as the direct pollutant emissions in the PM_{2.5} inversion. More importantly, current widely used AOD products are provided at coarse spatial resolutions (3–10 km) and show large estimation uncertainties over bright surfaces, especially over heterogeneous urban areas (He et al., 2017; Li et al., 2019a; Liu et al., 2019b; Wang et al., 2019; Wei et al., 2018a, 2018b, 2019c, 2019d). Therefore, the corresponding PM_{2.5} estimates are severely limited in application over small-scale areas.

Previous studies have mainly focused on exploring new approaches to improve the overall accuracy of PM_{2.5} concentrations for those years with a sufficient number of measurements from PM_{2.5} ground monitoring stations. These models showed skill in estimating PM_{2.5} for the current year, but most did not have an adequate predictive ability to generate long-term historical PM_{2.5} data records. A few studies have tried to reconstruct historical PM_{2.5} data across China using traditional approaches. However, the PM_{2.5} predictions were less accurate with overall low accuracies ($R^2 = 0.41\text{--}0.55$) at coarse spatial resolutions due to the limitations of the models themselves and data sources (Hammer et al., 2020; Lin et al., 2018; Ma et al., 2016; Xue et al., 2019). More accurate methods that improve the prediction accuracy of PM_{2.5} concentrations are thus needed to construct a historical PM_{2.5} dataset. This would make up for the gap in studies on PM_{2.5} variations across China. Therefore, long-term time series and high-quality PM_{2.5} datasets are

urgently needed for future studies on climate change and human health (Hong et al., 2019; Li et al., 2017a, b, c, 2019a,b, c; Xue et al., 2019).

Here, our objective is to develop a more advanced approach to improve the overall accuracy of PM_{2.5} estimates at a higher spatial resolution and then reconstruct historical PM_{2.5} data for China. For this purpose, our proposed tree-based ensemble Space-Time Extra-Trees (STET) model (Wei et al., 2020) is adopted here to retrieve PM_{2.5} concentrations. The 1 km MODIS Multi-Angle implementation of Atmospheric Correction (MAIAC) aerosol product (MCD19A2), newly released in May 2018 (Lyapustin et al., 2018), is used in this study. Ancillary information on meteorological variables, land use, pollutant emissions, and population are involved in the model to improve PM_{2.5}-AOD relationships. Based on this, we produce for the first time a high-resolution and high-quality PM_{2.5} dataset for China (i.e., China-HighPM_{2.5}), reconstructing the period from 2000 to 2018. We also perform a comprehensive investigation of spatiotemporal PM_{2.5} variations across China.

2. Materials and methods

2.1. Data sources and integration

2.1.1. In situ PM_{2.5} data

Hourly PM_{2.5} in situ observations from 2013 to 2018 were obtained from the China National Environmental Monitoring Center. They are measured using the tapered element oscillating microbalance (TEOM) or the β -attenuation method with a precision of ± 1.5 or $0.1 \mu\text{g}/\text{m}^3$, respectively (Xin et al., 2015). For air pollution monitoring, the number of observation stations has increased across China, going from 835 in 2013 to up to 1583 by the end of 2018 (Fig. 1). These stations are roughly evenly distributed throughout China and cover most natural and human conditions, especially in eastern China (~ 1289 stations) with a high concentration of industrial activities. In addition, there are 168, 184, 95, and 107 monitoring stations located in the Beijing-Tianjin-Hebei (BTH) region (113.1°E – 120.1°E , 35.8°N – 42.9°N), the Yangtze River Delta (YRD) region (117.2°E – 122.9°E , 28.5°N – 33.5°N), the Pearl River Delta (PRD) region (110.7°E – 116.5°E , 20.8°N – 25.8°N), and the Sichuan Basin (SCB) region (102.6°E – 108.4°E , 27.7°N – 32.6°N), respectively. In this study, problematic or singular values caused by instrument malfunction and calibration were first excluded (Guo et al., 2009). Daily PM_{2.5} values were then averaged from valid hourly observations for each year at each monitoring station in China.

2.1.2. MAIAC AOD products

The MODIS Collection 6 MAIAC AOD product (MCD19A2) at a 1 km resolution (Lyapustin et al., 2018) was used as the most important predictor of PM_{2.5}. Both Terra and Aqua MAIAC daily gridded AOD products covering mainland China were collected from 24 February 2000 for Terra and 4 May 2002 for Aqua, to 31 December 2018. The MAIAC 1 km AOD retrievals were validated against the Aerosol Robotic Network (AERONET) AOD measurements collected at 38 monitoring stations (Fig. 1) using the spatiotemporal matching method (Wei et al., 2019c), and compared with the widely used MODIS 10 km Dark Target (DT), Deep Blue (DB), and combined DT and DB (DTB) AOD retrievals from 2000 to 2018 in China (Fig. S1). The MAIAC AODs are highly consistent with the AERONET AODs (correlation coefficient, $R = 0.943$), with a mean absolute error (MAE) of 0.081, a root-mean-square error (RMSE) of 0.148, and $\sim 81\%$ of the data samples falling within the expected error window [$\pm (0.05 + 20\%)$]. More importantly, the number of retrievals is 1.5–2.6 times more, and the spatial resolution is 3–10 times higher than the widely used MODIS DT, DB, and DTB products in China. Other studies have also reported the same conclusions (Liu et al., 2019b; Tao et al., 2019; Wei et al., 2019c; Zhang et al., 2019b). Therefore, the most accurate, highest resolution, and widest coverage MODIS MAIAC AOD products were employed in our study. Both Terra and Aqua MAIAC AOD products were also averaged and

combined to further expand the spatial coverage so that more complete PM_{2.5} maps of China can be generated (Wei et al., 2020).

2.1.3. Auxiliary data

Auxiliary data, including meteorological variables, surface conditions, pollutant emissions, and population distributions, potentially affecting PM_{2.5} concentrations, were collected to improve PM_{2.5}-AOD relationships in China. In this study, several main meteorological variables, including temperature (TEM), relative humidity (RH), precipitation (PRE), evaporation (ET), surface pressure (SP), wind speed (WS), and wind direction (WD), were extracted from the ERA-Interim reanalysis (Dee et al., 2011). ERA-Interim boundary layer heights (BLH), generally consistent ($R = 0.8$) with those from radiosonde observations in China (Guo et al., 2016), are employed to account for aerosol vertical distributions. ERA-Interim products provide meteorological information from 1979 onward every 3 to 6 h at a spatial resolution of up to $0.125^\circ \times 0.125^\circ$. More importantly, they have been shown to be more reliable than many other atmospheric reanalysis products in China (Zhou and Wang 2016; Zhou et al., 2018).

The MODIS 1 km monthly Normalized Difference Vegetation Index (NDVI) product, the 500 m annual land-use cover (LUC) product, and the Shuttle Radar Topography Mission (SRTM) 90 m Digital Elevation Model (DEM) were also collected to reflect the current state of and change in the earth's surface. Multi-resolution Emission Inventory for China (MEIC) emissions, including aerosol precursors (i.e., NH₃, NO_x, and SO₂) and fine-sized particles (PM), generated from climate and chemical transport models at a spatial resolution of $0.25^\circ \times 0.25^\circ$ on a monthly basis, were selected to describe PM_{2.5} compositions and variations in China (Li et al., 2017c; Zhang et al., 2007). In addition, the 1 km annual LandScan™ population distribution (POP) product was selected to represent the population distribution in China (Dobson et al., 2000). Table S1 provides detailed information and access addresses of all data sources used in our study. Finally, all the above-mentioned independent variables were resampled to a uniform 1 km resolution.

2.2. Space-Time Extra-Trees model

Different from traditional decision trees and random forests, a tree-based ensemble learning approach, i.e., extremely randomized trees (extra-trees, Geurts et al., 2006), was selected for this study. The extra-trees model yields stronger selection randomness in features, parameters, models, and splits than other tree-based machine learning approaches, e.g., decision tree, random forest, and gradient boosting. The extra-trees model used in our study mainly consists of four steps:

- 1) Sample selection. Given the original data set D , the sample size N , and the feature number M , all data samples are used for model training in each base classifier in the classification model of extra-trees;
- 2) Feature selection. To enhance the randomness, m features are randomly selected from M features when each node is split, and the optimal feature is selected for node splitting at each node without pruning;
- 3) Extra-tree construction. The split sample subsets repeat Step (2) until a decision tree is generated according to the Classification And Regression Tree (CART) algorithm. Then repeat Steps (1) and (2) for K iterations to generate K decision trees. Finally, the extra-trees are built;
- 4) Final result output. The extra-trees are used to generate prediction results with test samples, and the prediction results of all base classifiers are counted. The final result is determined based on the average value of the outputs of all decision trees.

Geurts et al., (2006) provided a detailed description of the extra-trees algorithm. For the feature selection, the model is optimized by selecting more important variables to overcome the overfitting issue from using

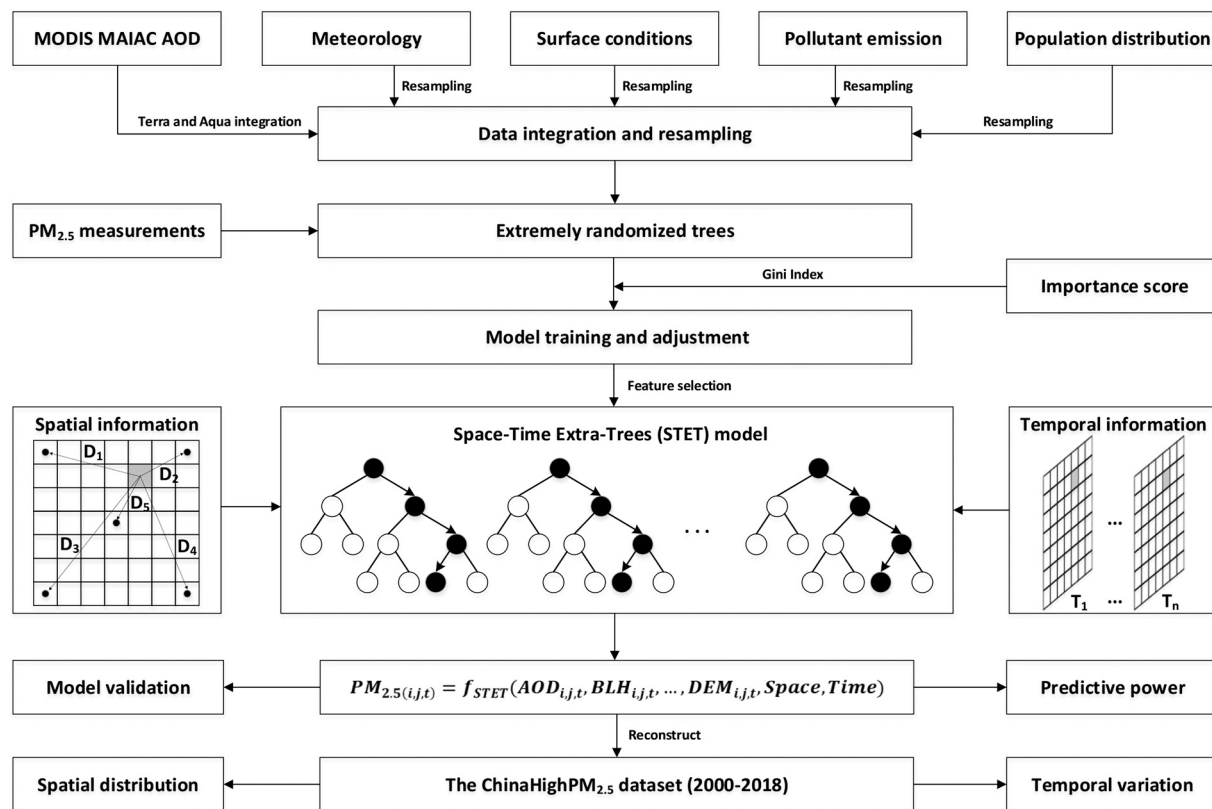


Fig. 2. Flowchart of the production of the ChinaHighPM_{2.5} dataset in this study.

redundant input variables. This can also both improve the overall accuracy and operational efficiency of the model. Therefore, the optimal combination of features is determined through a two-stage model training. In the first stage of model training, all the above-mentioned independent variables are input into the model. The more important features are selected according to the importance score calculated using the Gini Index (Jiang et al., 2009) when the model training is finished. Note that this score only represents the importance of each variable to the PM_{2.5} estimation in the extra-trees generation and does not represent the physical contributions.

Results show that the AOD is the most crucial indicator with the largest importance score of ~31% (Fig. S2). Seven meteorological variables (i.e., BLH, ET, TEM, RH, SP, WS, and WD) have noticeable effects on the PM_{2.5} estimation. Two main land surface variables, i.e., DEM and NDVI, and two main emission variables, i.e., NH₃ and PM, are also important. The remaining five variables are less important with small importance scores (< 2%) and excluded. Therefore, these 12 more important variables are used as inputs to the extra-trees model for re-training to establish robust PM_{2.5}-AOD relationships in the second stage.

Due to the spatiotemporal heterogeneity in PM_{2.5} distributions and variations, spatial and temporal information that most previous studies have neglected are introduced into the extra-trees model, and we thus refer to it as the Space-Time Extra-Trees (STET) model (Wei et al., 2020). Different from our previous study, the determination of spatiotemporal information is further improved. The space term is refined to include the longitude, latitude, and five Haversine distances of one point to the upper-left (D_1), upper-right (D_2), lower-left (D_3), and lower-right (D_4) corners, and the time term is simplified, represented by the day of the year (T_n). They are used to comprehensively describe the geolocation and mark the temporal difference of a given pixel point on a sphere, respectively. Lastly, the STET model is used to generate a high-resolution (1 km) and high-quality PM_{2.5} dataset for China (i.e., ChinaHighPM_{2.5}) over most of the period covered by Terra and Aqua MODIS measurements, i.e., 2000 to 2018. Fig. 2 shows the flowchart of the production of the ChinaHighPM_{2.5} dataset in this study.

2.3. Evaluation and analysis methods

The model performance was evaluated using the widely used 10-fold cross-validation (CV) approach (Rodriguez et al., 2010). Training and validation of the model were conducted over the period when the bulk of ground-based measurements of PM_{2.5} began in 2013. For the spatial analysis, monthly, seasonal, and annual mean PM_{2.5} data were generated from daily PM_{2.5} values for each grid cell using our previous data synthesis method (Wei et al., 2020). The spatial coverage of PM_{2.5} maps across China was calculated using the area-weighting approach by multiplying the cosine of latitude to minimize the effects of the earth's curvature. For the analysis of temporal variations, monthly mean PM_{2.5} concentrations were first deseasonalized by calculating the monthly anomalies to minimize the effects of the annual cycle. The linear trends were then derived from deseasonalized monthly PM_{2.5} anomalies using

Table 1
Summary of the ChinaHighPM_{2.5} dataset.

Parameter	ChinaHighPM _{2.5} dataset
Domain	[73.6°E, 134.8°E], [15.8°N, 53.7°N]
Data level	Level 2 Level 3
Temporal resolution	Daily Monthly Seasonal Annual
Temporal range	2013–2018 March 2000 to December 2018
Spatial resolution	0.01° × 0.01° (~ 1 km × 1 km)
Valid range	[0,1000]
Fill value	–999
Units	μg/m ³
Data type	Float
Creation date	ISO-8601
Data format	NetCDF (.nc filename extension)

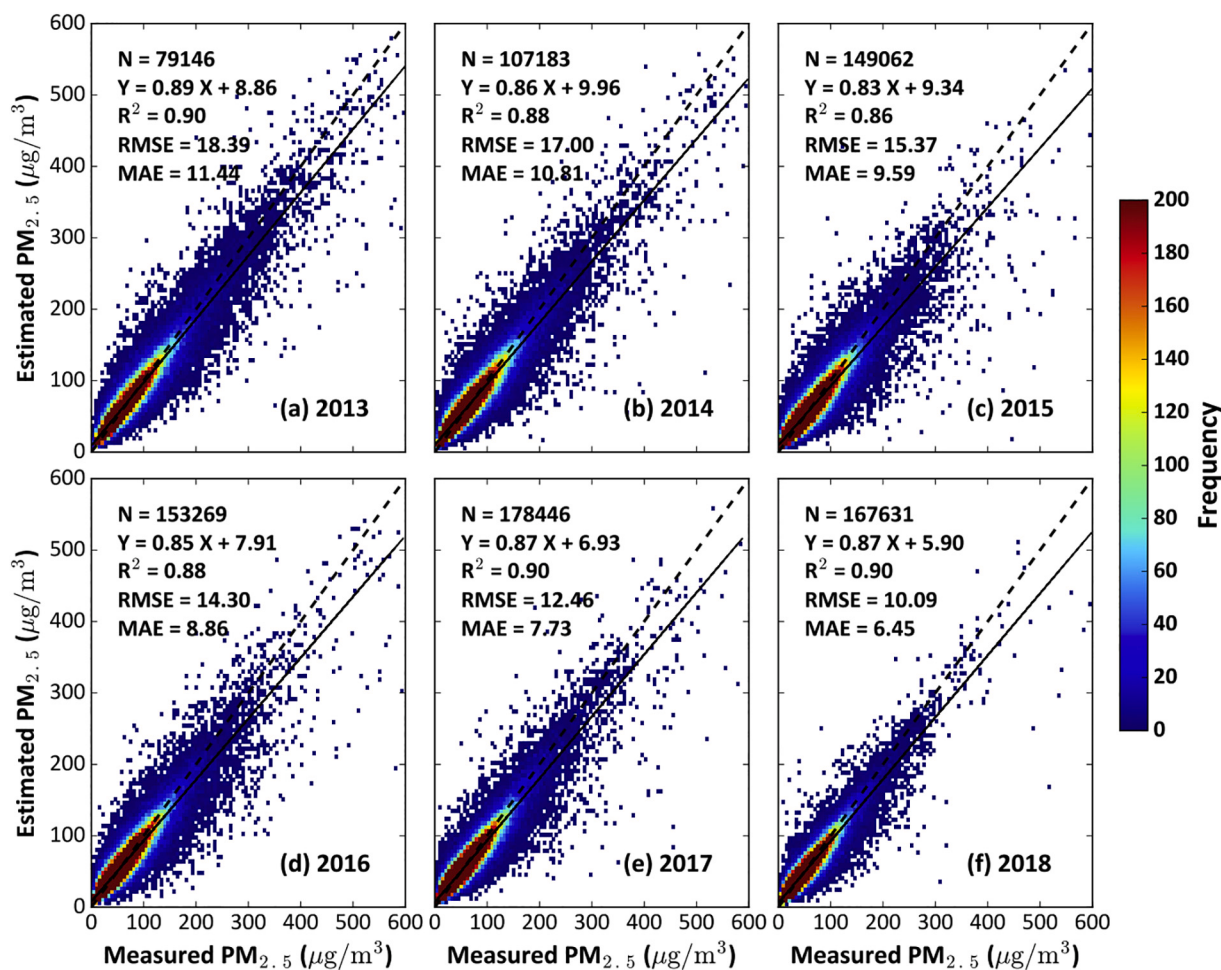


Fig. 3. Density scatterplots of cross-validation results of daily PM_{2.5} estimates for each year from 2013 to 2018 across China. Dashed lines denote 1:1 lines, and solid lines denote best-fit lines from linear regression. The sample size (N), coefficient of determination (R^2), root-mean-square error (RMSE), and mean absolute error (MAE) are also given. Units for RMSE and MAE are $\mu\text{g}/\text{m}^3$.

the ordinary least-squares-fitting approach, and the statistical significance of the linear trends was validated using the two-tailed test (Wei et al., 2019e).

3. Results and discussion

3.1. ChinaHighPM_{2.5} dataset

Applying the STET model to the large volume of input datasets, we reconstructed the historical high-resolution (1 km) and high-quality PM_{2.5} product in China, i.e., ChinaHighPM_{2.5} (released on 12 November 2019). Table 1 and Fig. S3 summarize the main features and provide an example of the NetCDF file contents, respectively, of the dataset. The ChinaHighPM_{2.5} dataset is arguably the first high-spatial-resolution (i.e., 1 km), longest-term (i.e., 2000–2018) dataset with relatively high accuracy across mainland China (74°E–135°E, 16°N–54°N). Per our inventory of previous similar related studies (Table S2), their PM_{2.5} products cover much shorter periods (mostly one to two years), lower accuracies (mostly CV- $R^2 < 0.8$), and much coarser resolutions (3–10 km). This ChinaHighPM_{2.5} dataset includes daily data from 1 January 2013 to 31 December 2018, and monthly data from March 2000 to December 2018. Seasonal and annual PM_{2.5} data were also synthesized and provided from 2000 to 2018. Note that this dataset is being continuously updated.

3.2. Evaluation of model performance

3.2.1. Overall accuracy

Fig. 3 shows the overall CV results of all daily PM_{2.5} estimates from all monitoring stations for each year in mainland China. Thanks to the rapid expansion of the PM_{2.5} observation network across China, the data volume used in our study has increased dramatically (from 79,146 samples in 2013 to 178,446 samples in 2017). In general, daily PM_{2.5} estimates derived from the STET model agree well with ground-based PM_{2.5} measurements (i.e., CV- $R^2 = 0.86$ –0.90), with average RMSE and MAE values ranging from ~10.0 to 18.4 $\mu\text{g}/\text{m}^3$ and ~6.4 to 11.5 $\mu\text{g}/\text{m}^3$, respectively, among different years at the national scale. Most data samples are evenly scattered around the 1:1 line, with strong slopes (~0.83–0.89) and small intercepts (~−5.9–10.0 $\mu\text{g}/\text{m}^3$), especially for the range with the largest data density (~0–150 $\mu\text{g}/\text{m}^3$). Furthermore, the STET model shows superior performance in PM_{2.5} estimates compared to most models developed in previous studies for the same study period focused on China (Table S2). However, the estimation uncertainty (e.g., RMSE and MAE) of PM_{2.5} decreased overall over the years, mainly because of the decreasing numerical ranges of data samples due to the improved air quality, and the increasing number of PM_{2.5} ground monitoring stations in recent years in China.

While the accuracy of our PM_{2.5} product is arguably the highest among peer products (Table S2), it still suffers from considerable uncertainties due to some inherent limitations, especially concerning aerosol vertical distributions. The BLH is the sole factor linking aerosol

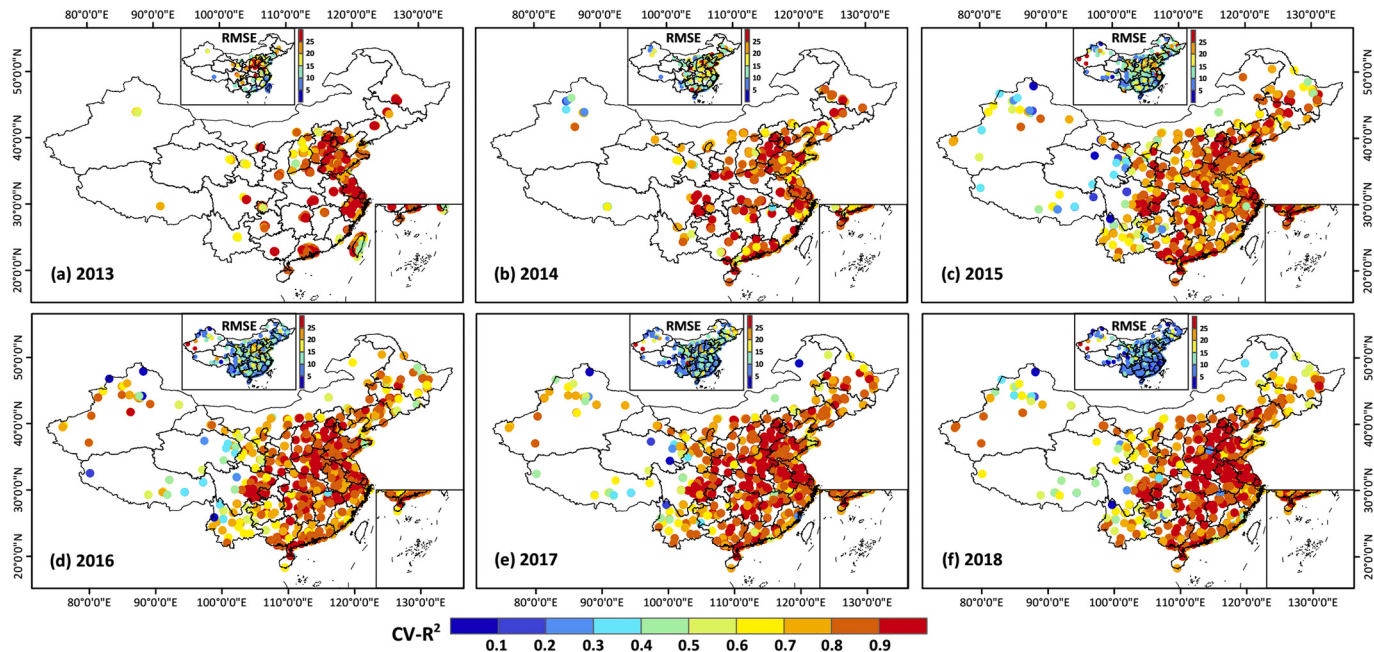


Fig. 4. Spatial distributions of the cross-validation coefficient of determination ($CV-R^2$) of daily $PM_{2.5}$ estimates from 2013 to 2018 at each monitoring station in China. Inset figures show the uncertainty (i.e., RMSE, $\mu\text{g}/\text{m}^3$) of $PM_{2.5}$ estimates.

column loading, denoted by the AOD, with surface $PM_{2.5}$ concentrations. Information on aerosol vertical distributions is critical to AOD- $PM_{2.5}$ relationships, especially for regions away from the sources of aerosol emissions (Toth et al., 2014, 2019). To account for the aerosol vertical distribution, we attempted to incorporate the Cloud-Aerosol Lidar and Infrared Pathfinder Satellite Observation (CALIPSO) monthly climatology of aerosol vertical profiles, noting that the instantaneous product has too sparse a coverage. It turns out to have little impact on the retrieval accuracy (Table S3) due to other inherent errors suffered by the CALIPSO (Misra et al., 2012; Pappalardo et al., 2010; Wu et al., 2014).

We also performed an uncertainty analysis of $PM_{2.5}$ estimates from

our STET model by varying the uncertainty of AOD as well as other variables from 1% to ~20% based on the validation results of the MAIAC AOD product in China. Fig. S4 presents the absolute mean relative errors of $PM_{2.5}$ estimates incurred by the uncertainties of the input parameters. In general, our model is most sensitive to AOD, and a 1% estimation error in AOD can lead to a ~0.27% estimation error in $PM_{2.5}$. By contrast, the model is less sensitive to other parameters, as denoted by the different slopes ranging from 0.01 to 0.05. The uncertainty analyses suggest that our model is relatively stable and robust, benefitting from the strong anti-noise ability of ensemble learning approaches (Breiman 2001; Geurts et al., 2006).

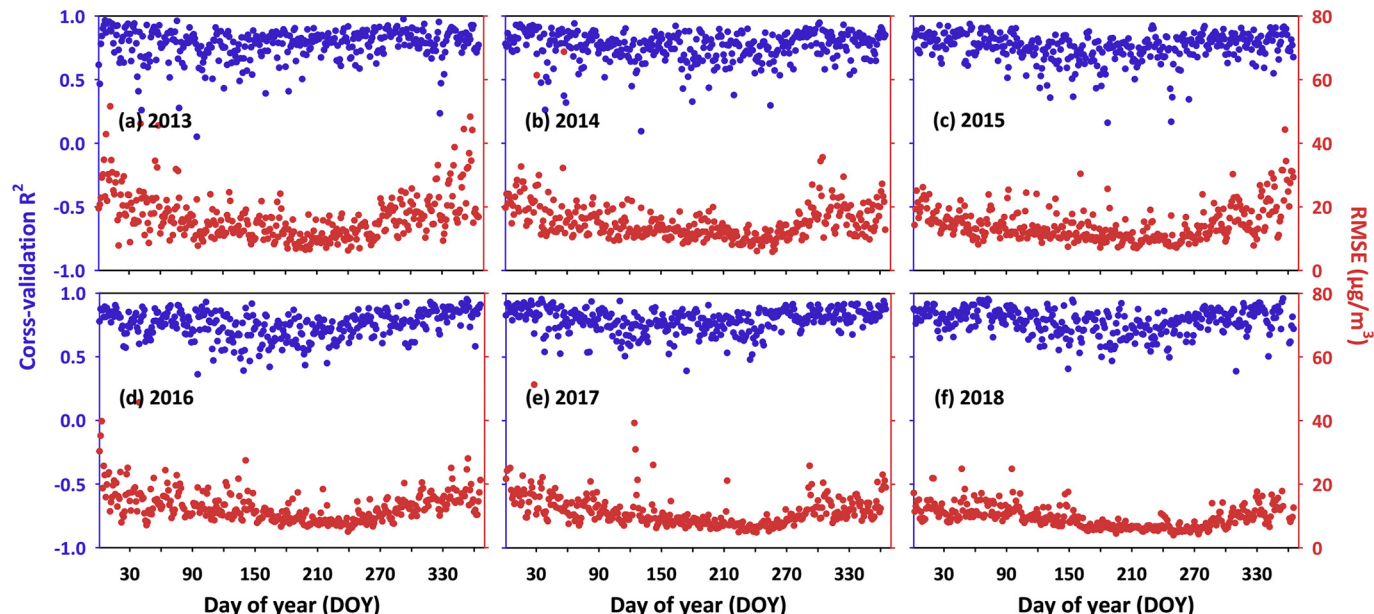


Fig. 5. Time series of the cross-validation coefficient of determination (R^2 , in blue) and uncertainty (i.e., root-mean-square error, or RMSE, in red) of daily $PM_{2.5}$ estimates as a function of the day of year from 2013 to 2018 across China. (For interpretation of the references to colour in this figure legend, the reader is referred to the web version of this article.)

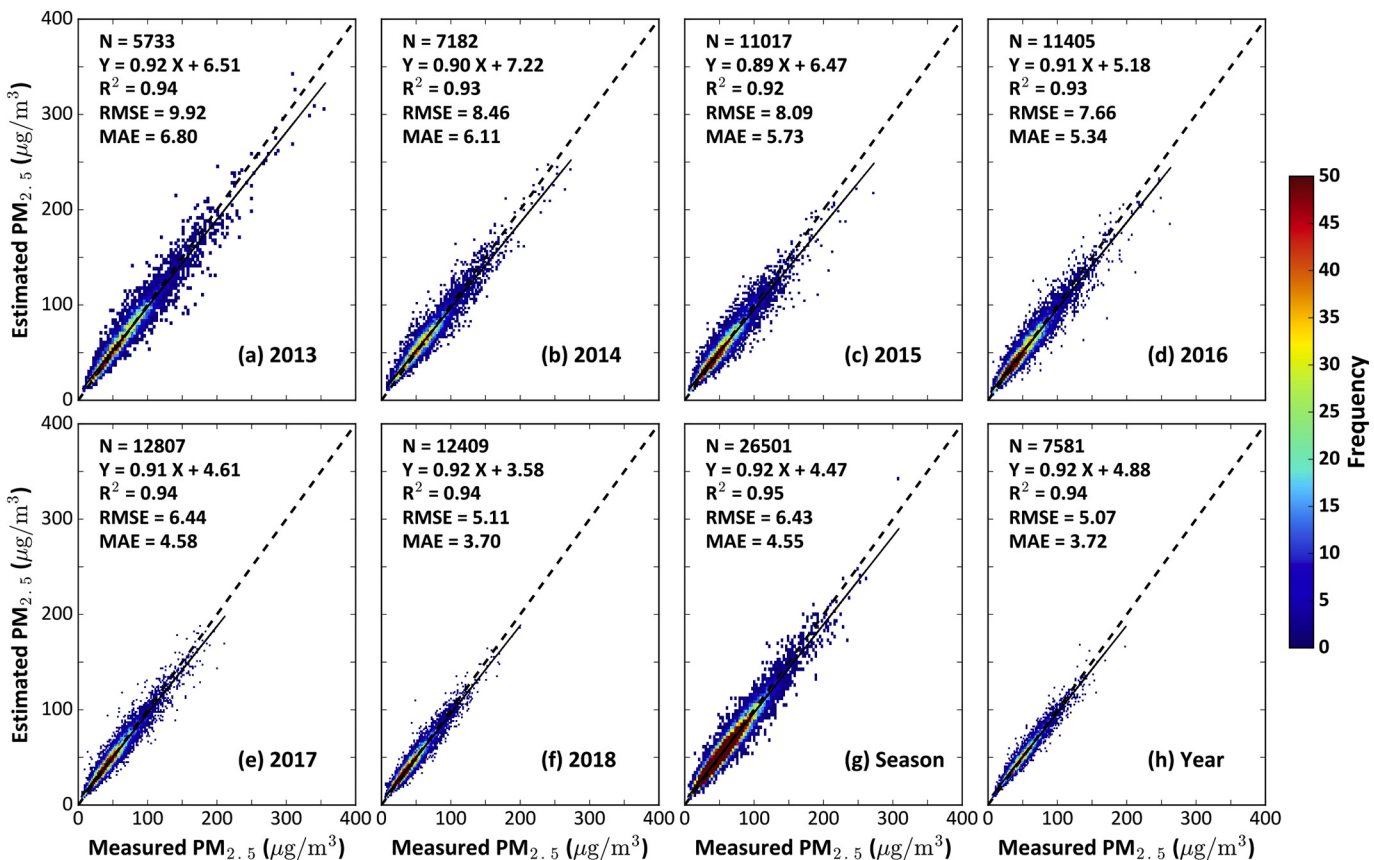


Fig. 6. Comparison of (a-f) monthly, (g) seasonal, and (h) annual synthetic PM_{2.5} estimates and observations from all monitoring stations for each year from 2013 to 2018 in China. Dashed lines denote 1:1 lines, and solid lines denote best-fit lines from linear regression. The sample size (N), coefficient of determination (R^2), root-mean-square error (RMSE), and mean absolute error (MAE) are also given. Units for RMSE and MAE are $\mu\text{g}/\text{m}^3$.

3.2.2. Spatiotemporal validation

Fig. 4 shows the spatial performance of the STET model in PM_{2.5} estimates from 2013 to 2018 across China. Here, only those stations with at least 10 matchups in each year were plotted and analyzed for statistical significance. The spatial patterns of the accuracy of the STET model are consistent from 2013 to 2018 across China but are heterogeneous with varying CV- R^2 values from site to site. The STET model performs best in central and eastern China, with most stations having high CV- R^2 values >0.9. By contrast, for several stations located in western China, the STET model performs poorly, with low average CV- R^2 values <0.4, possibly due to poor natural conditions and large estimation uncertainties in AODs (Wei et al., 2018a), as well as aerosol vertical distributions (Toth et al., 2014) over bright surfaces. Estimation errors are generally small, with RMSE values <10 $\mu\text{g}/\text{m}^3$ at most stations. Large estimation errors with RMSE values >20 $\mu\text{g}/\text{m}^3$ are observed at several stations located in the Xinjiang, Shanxi, and Hebei provinces, likely arising from frequent dust events or large amounts of pollutant emissions. In general, the average CV- R^2 value ranges from 0.82 to 0.87, and approximately 77–88% of the stations have CV- R^2 values >0.75 from 2013 to 2018 at the site scale in China.

Fig. 5 shows the temporal performance of the STET model in PM_{2.5} estimates at all monitoring stations as a function of the day of the year from 2013 to 2018 in China. Those days with less than 30 matchups for each year were not considered for statistical significance. The performance of our model is similar in each year from 2013 to 2018, with mean CV- R^2 values ranging from 0.75 to 0.79 on most days. Although CV- R^2 values were below 0.5 on some days, approximately 72–84% of the days have CV- R^2 values >0.7 from 2013 to 2018 in China. However, the uncertainty has an overall concave-upward parabolic trend in each year, with larger RMSE values >20 $\mu\text{g}/\text{m}^3$ in winter and smaller RMSE

values <10 $\mu\text{g}/\text{m}^3$ in summer, grossly proportional to the annual variation in the overall pollution level driven by emissions and depositions (Su et al., 2018, 2020). In general, the STET model can well capture daily PM_{2.5} variations, with small estimation errors throughout the year in China.

We also compared the monthly, seasonal, and annual synthetic PM_{2.5} estimates with ground-based measurements (Fig. 6). The monthly PM_{2.5} estimates are highly consistent with surface observations, e.g., R^2 (~0.92–0.94), slopes (~0.89–0.92), RMSE (~5.1–10.0 $\mu\text{g}/\text{m}^3$), and MAE (~3.7–6.8 $\mu\text{g}/\text{m}^3$) among different years from 2013 to 2018 (Fig. 6a-f). Although the retrieval errors vary year by year, the changes are so small that they do not significantly affect the trends. Taking the RMSE value as an example, it decreases and changes little, i.e., within $-1.5 \mu\text{g}/\text{m}^3$ per year. Furthermore, the seasonal and annual PM_{2.5} estimates are also highly consistent with ground measurements, with R^2 values of 0.95 and 0.94, same slope values of 0.92, average RMSEs of 6.43 $\mu\text{g}/\text{m}^3$ and 5.07 $\mu\text{g}/\text{m}^3$, and MAEs of 4.55 $\mu\text{g}/\text{m}^3$ and 3.72 $\mu\text{g}/\text{m}^3$ from 2013 to 2018, respectively (Fig. 6g-h). These results suggest that the ChinaHighPM_{2.5} product can provide reliable data for monitoring the spatial variation and temporal trend in PM_{2.5} pollution in China.

3.2.3. Predictive power

Since there are no monitoring stations before 2013, in this study, data from two years with different pollution conditions, were used to test the model's predictive power, i.e., the model built for one year was used to forecast PM_{2.5} concentrations in another year and validated with ground measurements made in this year. In addition, four traditional models, i.e., multiple linear regression (MLR), LME, GWR, and two-stage models, were selected to test their predictive power in estimating PM_{2.5} with the same data inputs as used in the STET model. Results show that

Table 2Comparison of the predictive powers of traditional models and the STET model to generate historical PM_{2.5} concentrations in China.

Model	Monthly			Seasonal			Year			Reference
	R ²	Slope	RMSE	R ²	Slope	RMSE	R ²	Slope	RMSE	
MLR	0.58	0.46	17.78	0.63	0.49	15.54	0.58	0.50	9.06	This study
LME	0.66	0.61	15.50	0.72	0.65	13.08	0.64	0.58	8.03	This study
GWR	0.68	0.63	15.71	0.75	0.67	13.24	0.75	0.75	7.64	This study
Two-stage	0.73	0.68	14.08	0.79	0.73	11.58	0.78	0.74	6.80	This study
Two-stage	0.73	–	–	0.79	–	–	–	–	–	Ma et al., 2016
CMAQ	0.54	0.85	26.40	–	–	–	0.53	1.00	19.70	Xue et al., 2019
ML	0.69	0.66	18.60	–	–	–	0.75	0.71	10.60	
ML + GAM	0.71	0.68	19.00	–	–	–	0.77	0.74	10.10	
STRF	0.73	0.65	14.88	0.78	0.70	11.42	0.79	0.72	8.08	Wei et al., 2019a
STET	0.80	0.83	11.26	0.81	0.87	9.59	0.82	0.84	6.10	This study

CMAQ: Community Multiscale Air Quality; GAM: generalized additive model; GWR: geographically weighted regression; LME: linear mixed-effect; ML: machine learning; MLR: multiple linear regression; STET: space-time extra-trees; STRF: space-time random forest.

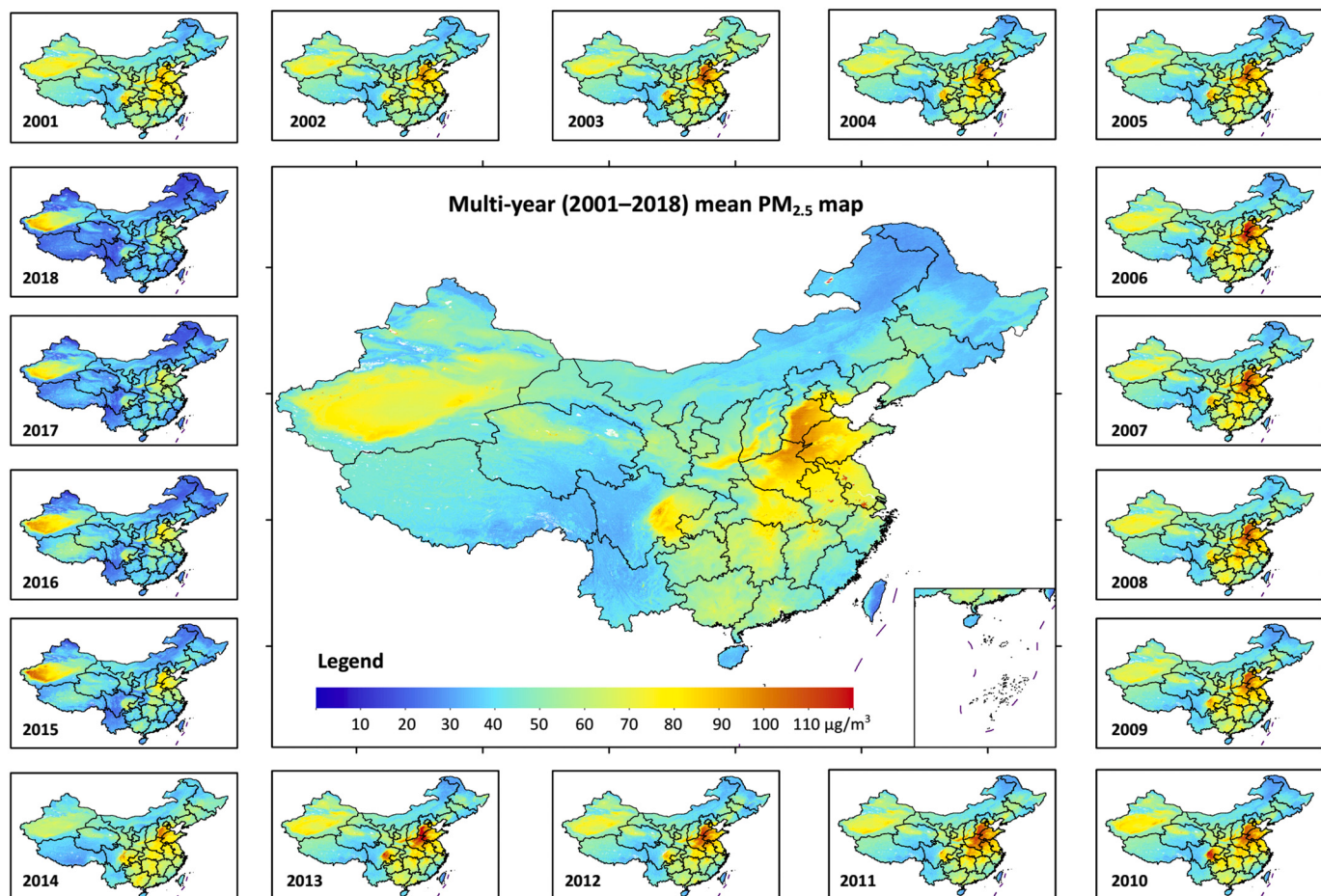


Fig. 7. MODIS-derived annual mean 1-km-resolution PM_{2.5} maps for each year from 2001 to 2018 in China.

the STET model can more accurately predict historical PM_{2.5} data records with small estimation uncertainties at monthly (i.e., R² = 0.80, slope = 0.83, and RMSE = 11.26 µg/m³), seasonal (i.e., R² = 0.81, slope = 0.87, and RMSE = 9.59 µg/m³), and annual (i.e., R² = 0.82, slope = 0.84, and RMSE = 6.10 µg/m³) scales than can traditional models (Table 2).

A few studies have explored the predictive power of their models in estimating historical PM_{2.5} concentrations, e.g., the two-stage model (Ma et al., 2016), Community Multiscale Air Quality (CMAQ) simulations (Xue et al., 2019), Machine Learning (ML) or ML + Generalized Additive Model (GAM) (Xue et al., 2019), and Space-Time Random Forest (STRF, Wei et al., 2019a). Table 2 shows that these models

predicted historical PM_{2.5} concentrations poorly at different temporal scales (Table 2). Our STET model shows a stronger predictive ability with reference to those models developed in previous studies. These results suggest that our model can capture historical PM_{2.5} concentrations in China more accurately, useful for reconstructing a long-term historical PM_{2.5} dataset.

3.3. Spatial coverage and distribution

3.3.1. National and regional pollution

Fig. 7 shows annual mean PM_{2.5} maps (1 km resolution) for each year from 2001 to 2018 across China and the multi-year mean PM_{2.5} map.

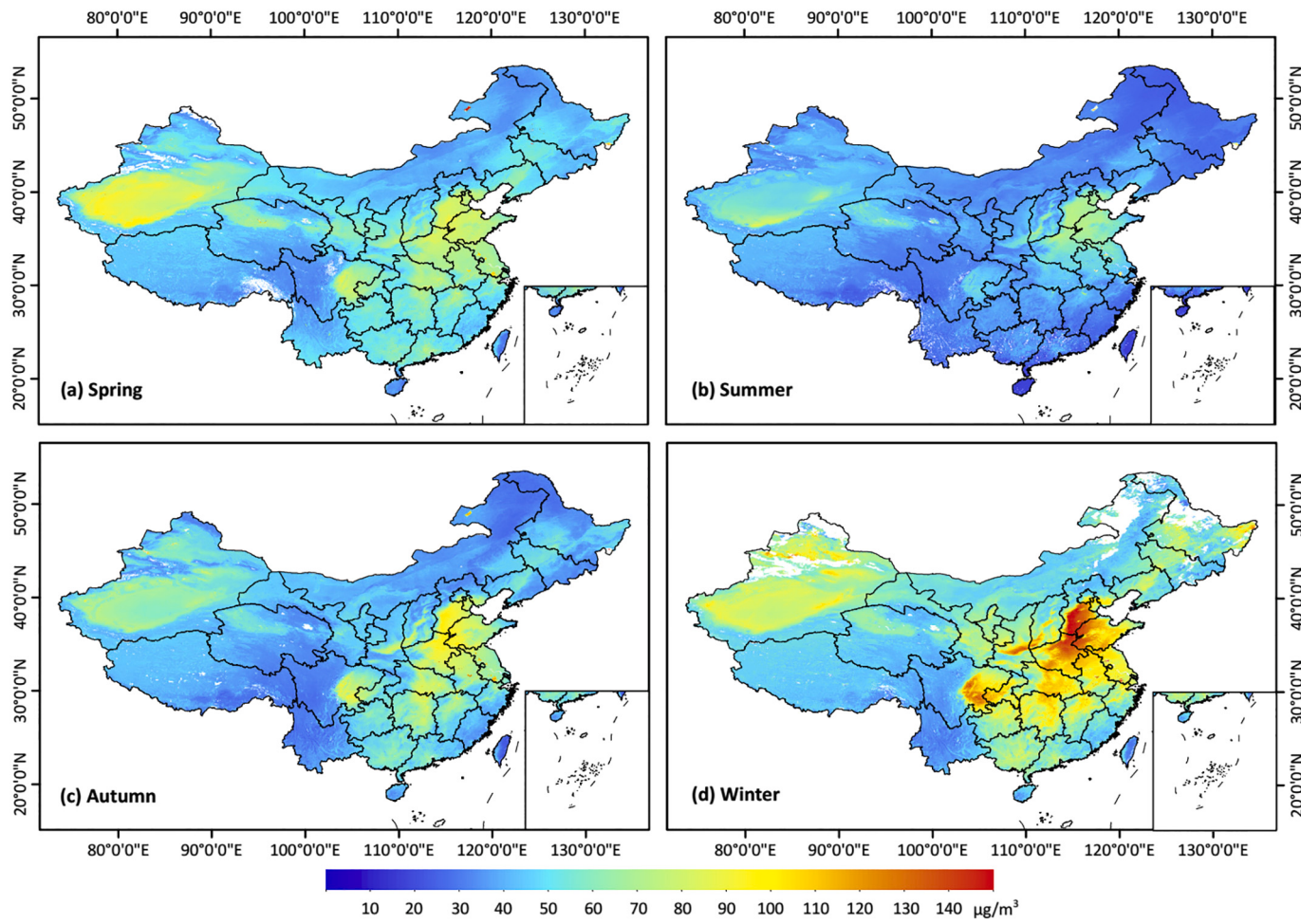


Fig. 8. MODIS-derived seasonal mean 1-km-resolution PM_{2.5} maps averaged over the period 2000–2018.

The STET model can estimate PM_{2.5} over more than 98% of the whole of China, a much wider spatial coverage than reported in previous studies, especially in western China. In general, spatial patterns are consistent among different years, where the highest PM_{2.5} values are found over Beijing, Tianjin, Hebei, Shaanxi, Henan, Shandong, Sichuan, and Xinjiang provinces, mainly due to intensive human activities, unique topographic conditions, and frequent dust events. PM_{2.5} values are overall low in other areas, especially southwest and northeast China. Multi-year mean PM_{2.5} concentrations are $49.4 \pm 14.2 \mu\text{g}/\text{m}^3$ for the whole of China, and $62.1 \pm 22.5 \mu\text{g}/\text{m}^3$, $63.0 \pm 11.1 \mu\text{g}/\text{m}^3$, $52.4 \pm 5.8 \mu\text{g}/\text{m}^3$, and $61.6 \pm 13.4 \mu\text{g}/\text{m}^3$ for the BTH, YRD, PRD, and SCB regions, respectively (Table S4). More importantly, more than 88% of the country suffers from a PM_{2.5} exposure risk, with an annual mean value exceeding the national air quality standard (i.e., PM_{2.5} = $35 \mu\text{g}/\text{m}^3$).

Fig. 8 illustrates the spatial distributions of seasonal mean PM_{2.5} concentration during 2000–2018 across China. The spatial patterns of PM_{2.5} concentration greatly differ at the seasonal level. In summer, PM_{2.5} pollution is the lightest, with most areas in China having PM_{2.5} values $<40 \mu\text{g}/\text{m}^3$ with an average value of $36.4 \pm 10.0 \mu\text{g}/\text{m}^3$, in particular, the PRD region ($\sim 31.6 \pm 6.4 \mu\text{g}/\text{m}^3$). By contrast, PM_{2.5} pollution is the most severe in winter, with much of China having PM_{2.5} values $>50 \mu\text{g}/\text{m}^3$ (average = $63.6 \pm 21.4 \mu\text{g}/\text{m}^3$), in particular, the BTH ($\sim 81.0 \pm 35.1 \mu\text{g}/\text{m}^3$), YRD ($\sim 82.2 \pm 14.6 \mu\text{g}/\text{m}^3$), and SCB ($\sim 88.5 \pm 24.1 \mu\text{g}/\text{m}^3$) regions (Table S4). Except for Xinjiang province, where dust events frequently occur, spring and autumn have similar spatial patterns and pollution levels from regional to national scales. However, 85–93% of China's expanse still exceeds the minimum acceptable air quality standard.

3.3.2. City-level pollution

Due to its high spatial resolution, the ChinaHighPM_{2.5} dataset allows for the examination of PM_{2.5} pollution at the city level. Fig. 9 shows zoom-in PM_{2.5} maps from 2000 to 2018 and the corresponding land-use-cover map for central China. In general, PM_{2.5} pollution is closely related to the land-use cover, where PM_{2.5} concentrations are $>80 \mu\text{g}/\text{m}^3$ in main urban and built-up areas (red colour in Fig. 9f) and croplands (yellow colour in Fig. 9f) due to more anthropogenic aerosols (e.g., pollutant emissions, coal, and agricultural burning), especially in winter. PM_{2.5} pollution is generally $<40 \mu\text{g}/\text{m}^3$ in forests and grasslands with abundant vegetation cover and sparse human activities. These findings illustrate that this new 1-km-resolution PM_{2.5} data is useful for studying air pollution in urban areas.

The frequency histograms of PM_{2.5} concentration based on data from 382 prefecture-level cities in China (Fig. S5) for different study periods and at different temporal scales are plotted in Fig. S6. PM_{2.5} values range from 10 to $140 \mu\text{g}/\text{m}^3$ at the city level among the different periods. 67–73% and 91–97% of the cities are exposed to moderate PM_{2.5} pollution levels ($\sim 40–80 \mu\text{g}/\text{m}^3$) and exceed the acceptable air quality standard, respectively, during the entire and first three periods. On the contrary, most cities in China from 2016 to 2018 have PM_{2.5} values $<60 \mu\text{g}/\text{m}^3$, and more than half of the cities (~57%) meet the acceptable air quality standard. Also seen are large differences at the city level on annual and seasonal scales. Most cities have similar PM_{2.5} distributions, with ~90–95% of them having pollution levels exceeding the acceptable air quality standard on an annual scale and in spring and autumn. The lowest PM_{2.5} pollution level is found in most cities in summer, with ~63% of them having pollution levels meeting the acceptable air quality

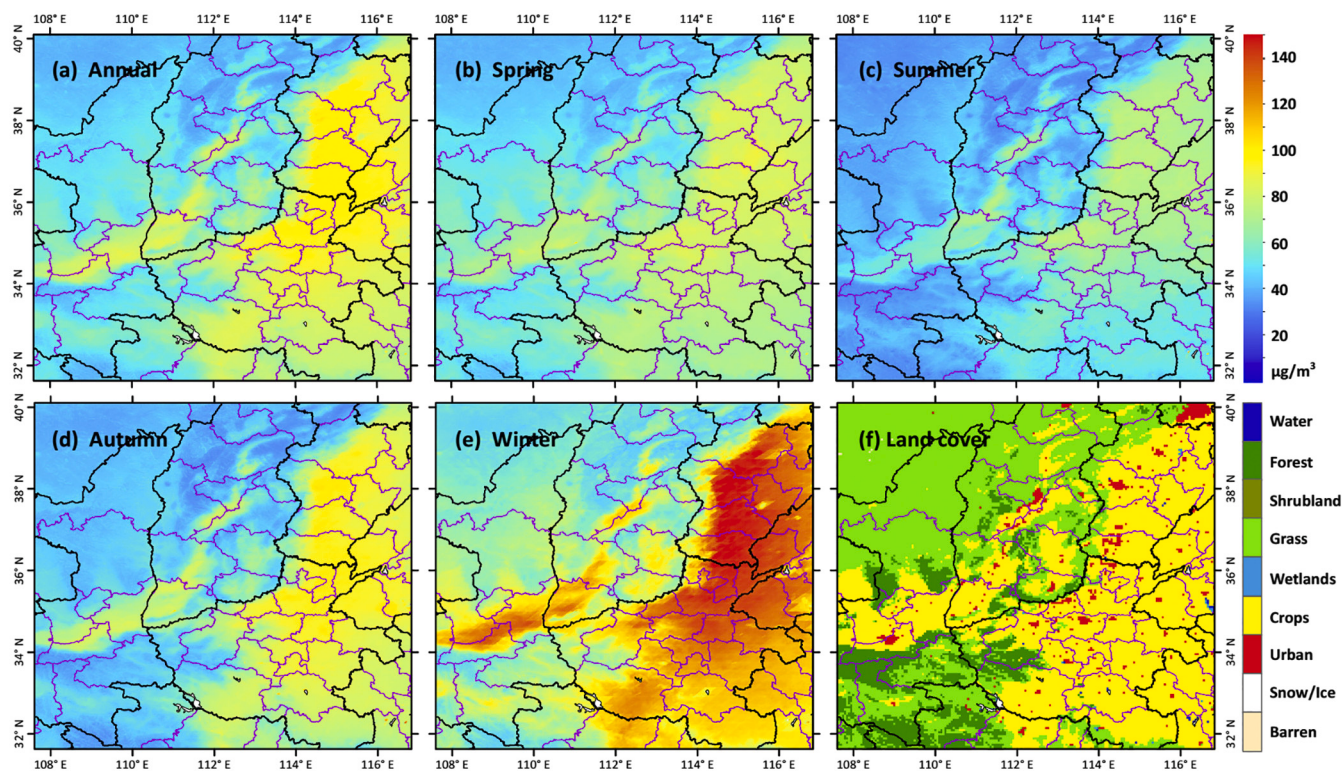


Fig. 9. Zoom-in maps of (a) annual and (b–e) seasonal mean 1-km-resolution PM_{2.5} maps averaged over the period 2000–2018, and (f) land-use type at the city level over central China, where black and pink lines represent provincial and city boundaries, respectively. (For interpretation of the references to colour in this figure legend, the reader is referred to the web version of this article.)

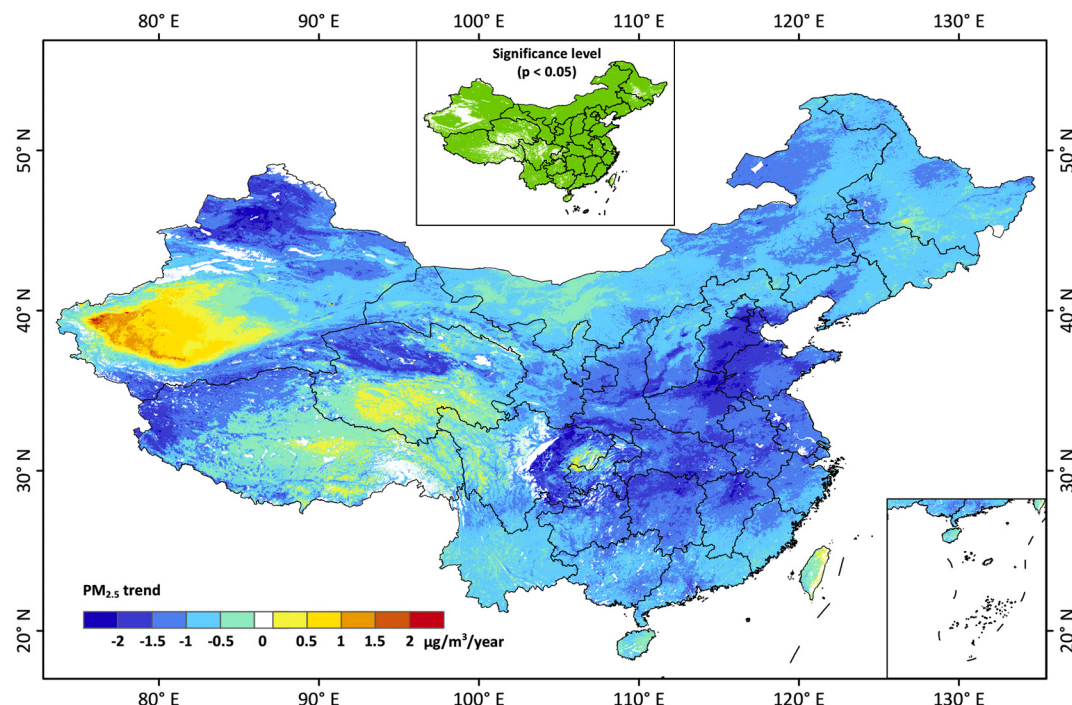


Fig. 10. Spatial distribution of linear PM_{2.5} trends ($\mu\text{g}/\text{m}^3/\text{yr}$) from 2001 to 2018 in China, where the green areas in the inset figure represent trends that are significant at the 95% ($p < 0.05$) confidence level. (For interpretation of the references to colour in this figure legend, the reader is referred to the web version of this article.)

Table 3

Statistics of annual and seasonal PM_{2.5} trends ($\mu\text{g}/\text{m}^3/\text{yr}$) and their significance levels (p) from 2000 to 2018 across China, in eastern China (ECHN), and four typical regions.

Region	Annual		Spring		Summer		Autumn		Winter	
	Trend	p	Trend	p	Trend	p	Trend	p	Trend	p
China	-0.89	< 0.001	-0.95	< 0.001	-0.89	< 0.001	-0.72	< 0.05	-0.67	< 0.05
ECHN	-1.09	< 0.001	-1.13	< 0.001	-0.99	< 0.001	-0.85	< 0.05	-0.82	0.11
BTH	-1.09	< 0.001	-1.12	< 0.001	-1.19	< 0.01	-0.85	< 0.05	-0.71	0.23
YRD	-1.24	< 0.001	-1.26	< 0.001	-1.03	< 0.01	-1.11	< 0.01	-0.94	0.13
PRD	-0.91	< 0.001	-0.66	0.13	-0.53	< 0.01	-0.79	0.087	-0.53	0.23
SCB	-1.46	< 0.001	-1.13	< 0.05	-0.98	< 0.01	-1.20	< 0.01	-1.32	0.07

BTH: Beijing-Tianjin-Hebei; PRD: Pearl River Delta; SCB: Sichuan Basin; YRD: Yangtze River Delta.

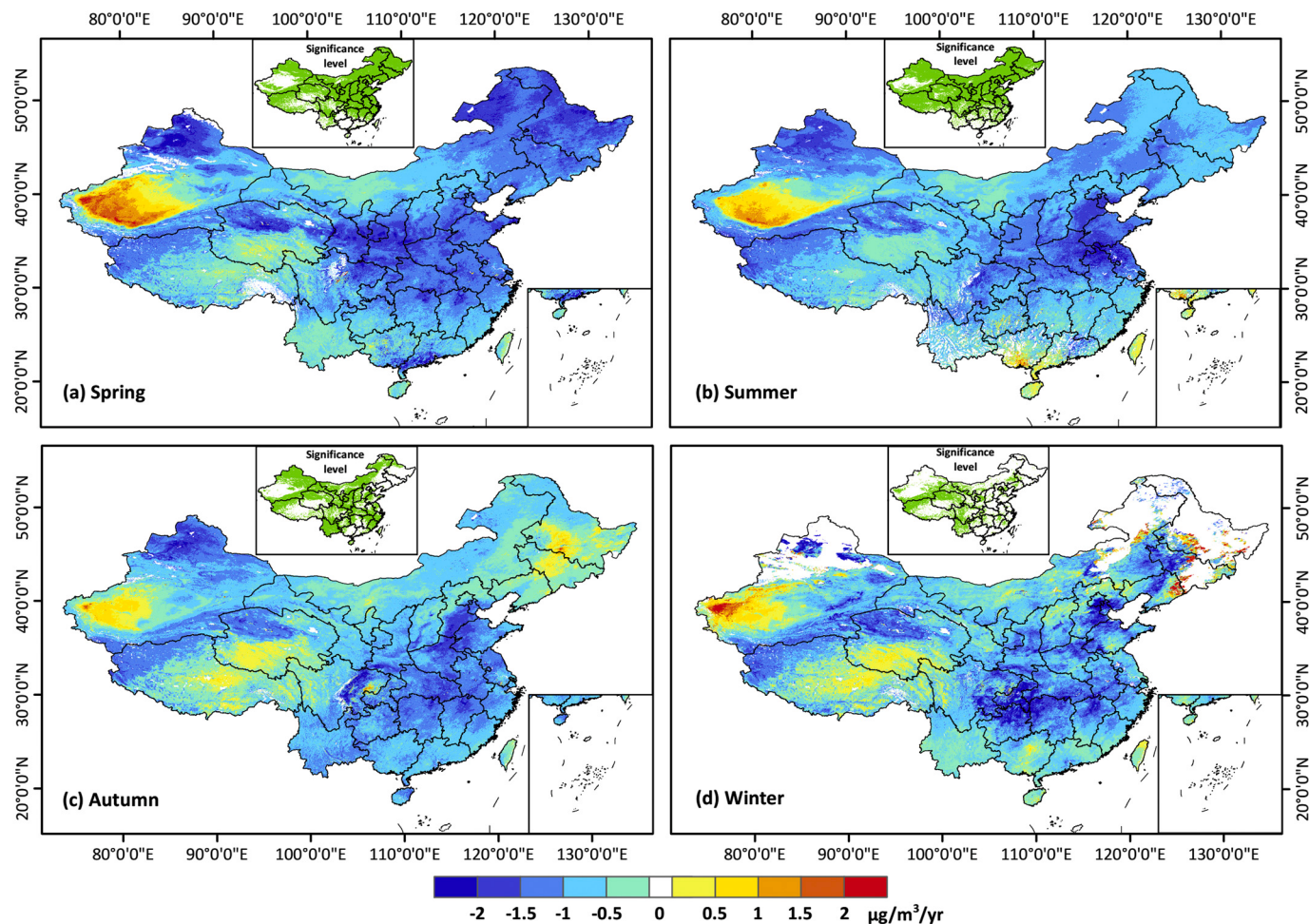


Fig. 11. Spatial distributions of seasonal PM_{2.5} trends ($\mu\text{g}/\text{m}^3/\text{yr}$) from 2000 to 2018 across China, where the green areas in the inset figures represent trends that are significant at the 95% ($p < 0.05$) confidence level. (For interpretation of the references to colour in this figure legend, the reader is referred to the web version of this article.)

standard. Most cities are exposed to the highest PM_{2.5} pollution levels in winter, with only 2% of the cities having pollution levels meeting the acceptable air quality standard. More importantly, ~32% of the cities face severe PM_{2.5} pollutions ($\text{PM}_{2.5} > 80 \mu\text{g}/\text{m}^3$).

3.4. Long-term variation and trend

3.4.1. National and regional trends

This section focuses on exploring historical spatiotemporal variations in PM_{2.5} pollution across mainland China. Fig. 10 plots the linear PM_{2.5} trends from 2001 to 2018 in China, and Table 3 summarizes the statistical results. PM_{2.5} pollution has significantly changed ($p < 0.05$)

over almost all of China's expanse from 2001 to 2018, with an average PM_{2.5} trend of $-0.89 \mu\text{g}/\text{m}^3/\text{yr}$ ($p < 0.001$). The variation trend of PM_{2.5} shows a pronounced geographic dependence. For example, the North China Plain has a decreasing PM_{2.5} trend of $>1.5 \mu\text{g}/\text{m}^3/\text{yr}$ ($p < 0.05$). Likewise, there are significant downward trends over the BTH ($\sim -1.09 \mu\text{g}/\text{m}^3/\text{yr}$, $p < 0.001$), YRD ($\sim -1.24 \mu\text{g}/\text{m}^3/\text{yr}$, $p < 0.001$), PRD ($\sim -0.91 \mu\text{g}/\text{m}^3/\text{yr}$, $p < 0.001$), and SCB ($\sim -1.46 \mu\text{g}/\text{m}^3/\text{yr}$, $p < 0.001$) regions from 2001 to 2018. By contrast, the Taklimakan Desert in Xinjiang province shows a significant increasing PM_{2.5} trend ($p < 0.05$). There are some areas in southwestern China showing increasing trends in PM_{2.5} concentration, but these trends are not statistically significant.

Fig. 11 shows seasonal PM_{2.5} trends from 2000 to 2018 across China.

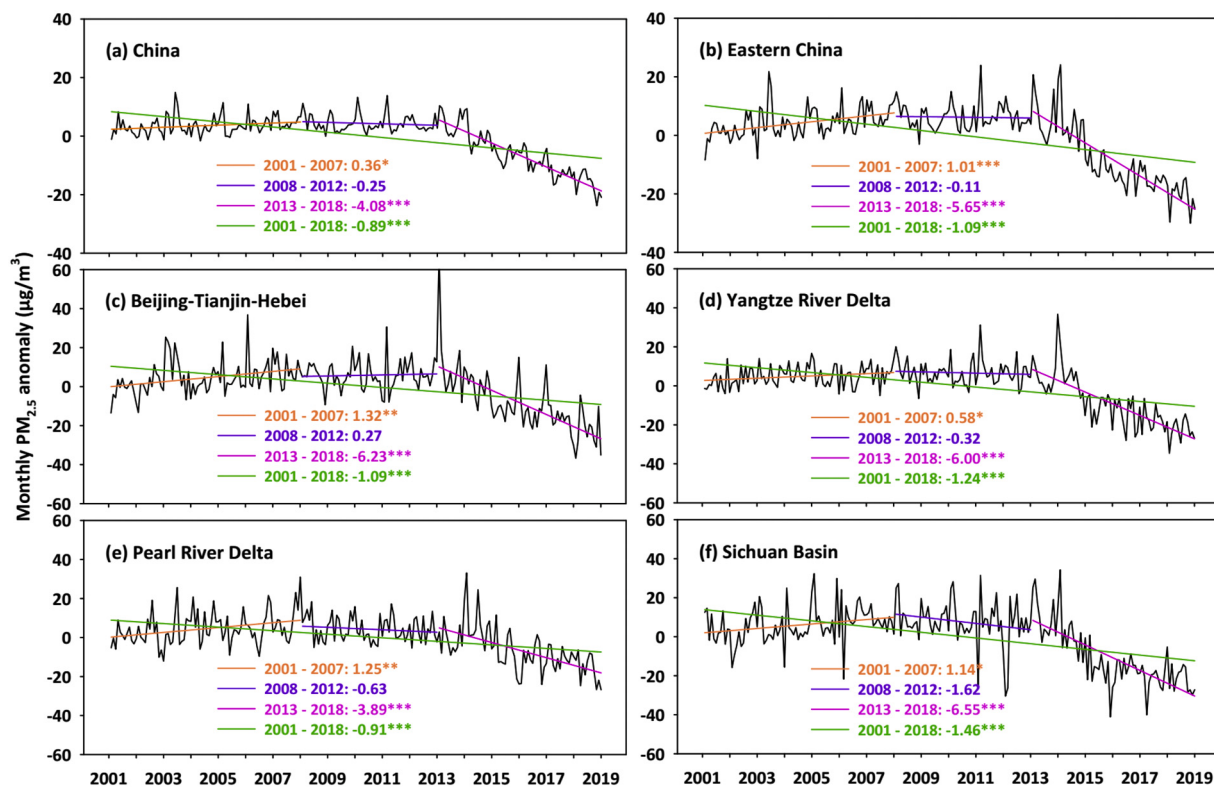


Fig. 12. Time series of monthly PM_{2.5} anomalies from 2001 to 2018 over (a) the whole of China, (b) eastern China, and (c-f) four typical regions. The different colored lines are the trend lines for different periods, where *, **, and *** represent trends that are significant at the 95% ($p < 0.05$), 99% ($p < 0.01$), and 99.9% ($p < 0.001$) confidence levels, respectively.

PM_{2.5} pollution has significantly decreased with an average trend of -0.95 ($p < 0.001$), -0.89 ($p < 0.001$), -0.72 ($p < 0.05$), and -0.67 ($p < 0.05$) µg/m³/yr in spring, summer, autumn, and winter, respectively (Table 3). However, there are differences in the seasonal variations at the regional level. In general, spring and summer have trends with similar spatial distributions across China. Except for southern and western China, the other regions show significant decreasing trends, especially the BTH, YRD, and SCB regions (< -1 µg/m³/yr, $p < 0.05$). In autumn, central, southeast, and southwest China are areas where PM_{2.5} significantly changed, although the change is much less than the changes during spring and summer. Most of China's areas show overall decreasing PM_{2.5} trends in winter, especially for some cities, e.g., Beijing and Tianjin (< -2 µg/m³/yr, $p < 0.05$). In Xinjiang province, overall increasing PM_{2.5} trends are seen in all seasons, especially in the Tarim Basin in spring (> 1 µg/m³/yr, $p < 0.05$), possibly suggesting an increasing number of sandstorms.

However, the increasing and decreasing trends could be offset over the long term, considering the watershed of around 2007 or 2008 when trends in most parts of China changed from increasing to decreasing. Considering major historical events that had a strong bearing on air quality in China (i.e., the Olympic Games and the Action Plan), our trend analyses are first divided into three periods to gauge their impact on national and regional PM_{2.5} pollution. Fig. 12 shows the time series of monthly PM_{2.5} anomalies from 2001 to 2018 over China, eastern China, and four typical regions. PM_{2.5} concentrations have an annual cycle, i.e., the maximum PM_{2.5} value is observed around January, and the minimum PM_{2.5} value is observed in July in any given year. In the early period of our study (2001–2007), PM_{2.5} had significantly increased by 0.3 to 1.4 µg/m³/yr ($p < 0.05$) across China (especially eastern China) and the four typical regions. The opposite was the case thereafter (2008–2012) for all regions but the BTH, with the sharpest decline in the last six years (2013–2018) across China (~ -4.08 µg/m³/yr, $p < 0.001$), especially in the BTH (~ -6.23 µg/m³/yr, $p < 0.001$), YRD (~ -6.00

µg/m³/yr, $p < 0.001$), and SCB (~ -6.55 µg/m³/yr, $p < 0.001$) regions.

Furthermore, trends are calculated for different time scales (from 3 to 18 years) and periods of varying beginning years until the end of 2018 with varying time lengths across China (Fig. 13). Note that PM_{2.5} trends are different during different periods and for different regions. PM_{2.5} pollution shows overall increasing trends before 2010, then significant decreasing trends ($p < 0.05$) since 2012 across China. There is a similar pattern in PM_{2.5} variations in eastern China but with larger values. The BTH and YRD regions have more consistent PM_{2.5} variations. The trends are significantly positive ($p < 0.05$) during the period 2001–2013, and smaller and relatively stable in the middle, separate periods, but significantly negative after 2013. Overall, PM_{2.5} concentrations increased before 2007 and 2005 in the PRD and SCB regions, respectively, then decreased, especially since 2013, when the largest trends occurred ($p < 0.05$). In general, the strongest trends are mainly concentrated in the lower-left and lower-right sections of each plot, suggesting that the trends can change rapidly over a short period. This highlights the importance of investigating spatiotemporal PM_{2.5} variations to identify “hot spots” of pollution and to understand their causes.

3.4.2. Relation to government policies

Although PM_{2.5} loadings differ from 2001 to 2018 due to the joint influence of both natural conditions and human activities, subtle differences among the years are barely visible (Fig. 7). Therefore, mean PM_{2.5} concentrations were calculated for four typical study periods (Fig. 14) and their differences with the mean PM_{2.5} level from 2001 to 2018 in China (Fig. S7). The spatial distributions of PM_{2.5} pollution are similar, with small differences over China and typical regions during the 10th (2001–2005) and 12th (2011–2015) FYP periods (Table S5). 70–90% of the areas have PM_{2.5} values that are slightly higher than the overall level of PM_{2.5} pollution during 2001–2018, and 91–96% of the areas have PM_{2.5} values exceeding the national air quality standard. During the 11th FYP (2006–2010), China experienced the most severe

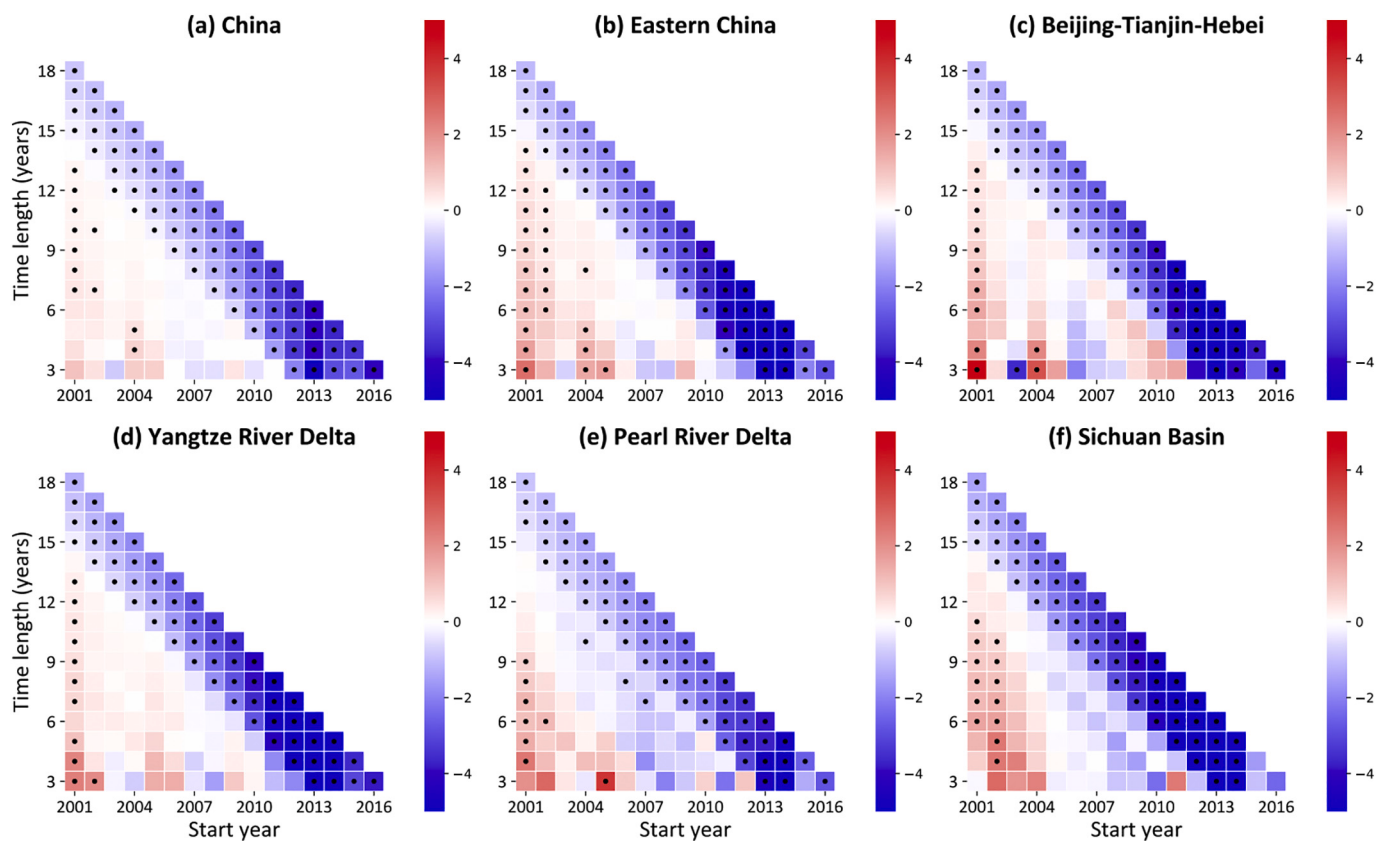


Fig. 13. Temporal PM_{2.5} trends ($\mu\text{g}/\text{m}^3/\text{yr}$) derived from deseasonalized monthly anomalies for different periods over China and typical regions, where the x-axis represents the start year, and the y-axis represents the time length (in years) since the start year. Black points indicate trends that are significant at the 95% confidence level ($p < 0.05$).

PM_{2.5} pollution levels, with the highest mean PM_{2.5} concentrations in most regions. Approximately 95% and 94% of the areas exceeded the average level and the air quality standard, especially the North China Plain and SCB, with larger differences $>10 \mu\text{g}/\text{m}^3$.

By contrast, during 2016–2018, PM_{2.5} pollution was at its lowest, with the lowest mean PM_{2.5} values and the largest differences with the overall average PM_{2.5} concentration. More than 95% of the areas have PM_{2.5} concentrations that are lower than the overall average PM_{2.5} concentration during 2001–2018, and 56% of the areas have PM_{2.5} values below the national air quality standard. In general, PM_{2.5} concentrations were high across China during the first few years and peaked around 2007, gradually decreasing to an overall low level in recent years (Fig. S8). The 2008 Olympic Games were, arguably, the major starting point in this turnaround due to the strong actions taken aimed at reducing pollution emissions prior to the Games (Du and Mendelsohn 2011; Shen et al., 2011).

Fig. 15 shows the spatiotemporal PM_{2.5} variations across China for different government policy periods. PM_{2.5} concentrations increased significantly over eastern China ($\sim 1.02 \mu\text{g}/\text{m}^3/\text{yr}$, $p < 0.05$) during the 10th FYP (2001–2005), especially over the YRD ($\sim 0.93 \mu\text{g}/\text{m}^3/\text{yr}$, $p < 0.05$) and PRD ($\sim 1.36 \mu\text{g}/\text{m}^3/\text{yr}$, $p < 0.05$) regions (Table 4). This was mainly due to the significant growth of the economy with an increasing gross domestic product rate of 13% per year, but without considering environmental protection. During the 11th FYP (2006–2010), however, most areas showed overall weak decreasing PM_{2.5} trends in China ($\sim -0.29 \mu\text{g}/\text{m}^3/\text{yr}$, $p = 0.24$) when pollution prevention measures began to take effect. These measures involved reforming industrial and energy structures at a time when the economic growth slowed somewhat but was still at a high rate of 11.2%.

During the 12th FYP (2011–2015), the air quality improved much more significantly across China ($\sim -2.70 \mu\text{g}/\text{m}^3/\text{yr}$, $p < 0.001$),

especially in the YRD ($\sim -4.33 \mu\text{g}/\text{m}^3/\text{yr}$, $p < 0.001$) and SCB ($\sim -5.24 \mu\text{g}/\text{m}^3/\text{yr}$, $p < 0.001$) regions, when more intensified adjustment and optimization of industrial and energy consumption structures took place, aiming at a more dramatic reduction in main pollution emissions, especially in key areas such as the BTH, PRD, and YRD regions. Moreover, the Qinghai Tibet Plateau also showed significant downward PM_{2.5} trends ($\sim -6 \mu\text{g}/\text{m}^3/\text{yr}$, $p < 0.05$), which may not be reliable, given the scarcity of monitoring stations. During the current FYP (2016–2020), PM_{2.5} pollution has continued to decrease by $4.26 \mu\text{g}/\text{m}^3/\text{yr}$ ($p < 0.001$) across China from 2016 to 2018, especially in eastern China ($\sim -3.07 \mu\text{g}/\text{m}^3/\text{yr}$, $p < 0.001$), and the BTH ($\sim -4.78 \mu\text{g}/\text{m}^3/\text{yr}$, $p < 0.01$) and YRD ($\sim -4.05 \mu\text{g}/\text{m}^3/\text{yr}$, $p < 0.01$) regions. Approximately 40%, 52%, 94%, and 96% of prefecture-level cities showed decreasing PM_{2.5} concentrations during the four FYPs, respectively, especially during the twelfth FYP when there was a large reduction in PM_{2.5} ($> 20\%$) at $\sim 75\%$ of the cities in China (Fig. S9).

During the Action Plan (2013–2017), PM_{2.5} pollution significantly declined over most areas in eastern China ($\sim -6.11 \mu\text{g}/\text{m}^3/\text{yr}$, $p < 0.001$), especially the BTH ($\sim -6.65 \mu\text{g}/\text{m}^3/\text{yr}$, $p < 0.001$), YRD ($\sim -6.51 \mu\text{g}/\text{m}^3/\text{yr}$, $p < 0.001$), PRD ($\sim -3.80 \mu\text{g}/\text{m}^3/\text{yr}$, $p < 0.001$), and SCB ($\sim -8.00 \mu\text{g}/\text{m}^3/\text{yr}$, $p < 0.001$) regions (Table 5). More importantly, the satellite-based trends of PM_{2.5} pollution derived from the STET model are highly consistent (i.e., differences within $\pm 1.5 \mu\text{g}/\text{m}^3/\text{yr}$) with those calculated from ground-based observations on all scales from city to regional to national scales in China, further attesting to the robustness of our retrievals. Their discrepancies are mainly caused by the different spatial coverages of in situ and satellite observations. The latter may increase with decreasing density of ground monitoring stations (e.g., the SCB).

In general, PM_{2.5} pollution had decreased by 32.7%, 32.5%, 36.3%, and 31.5% across China and three key regions (i.e., BTH, YRD, and

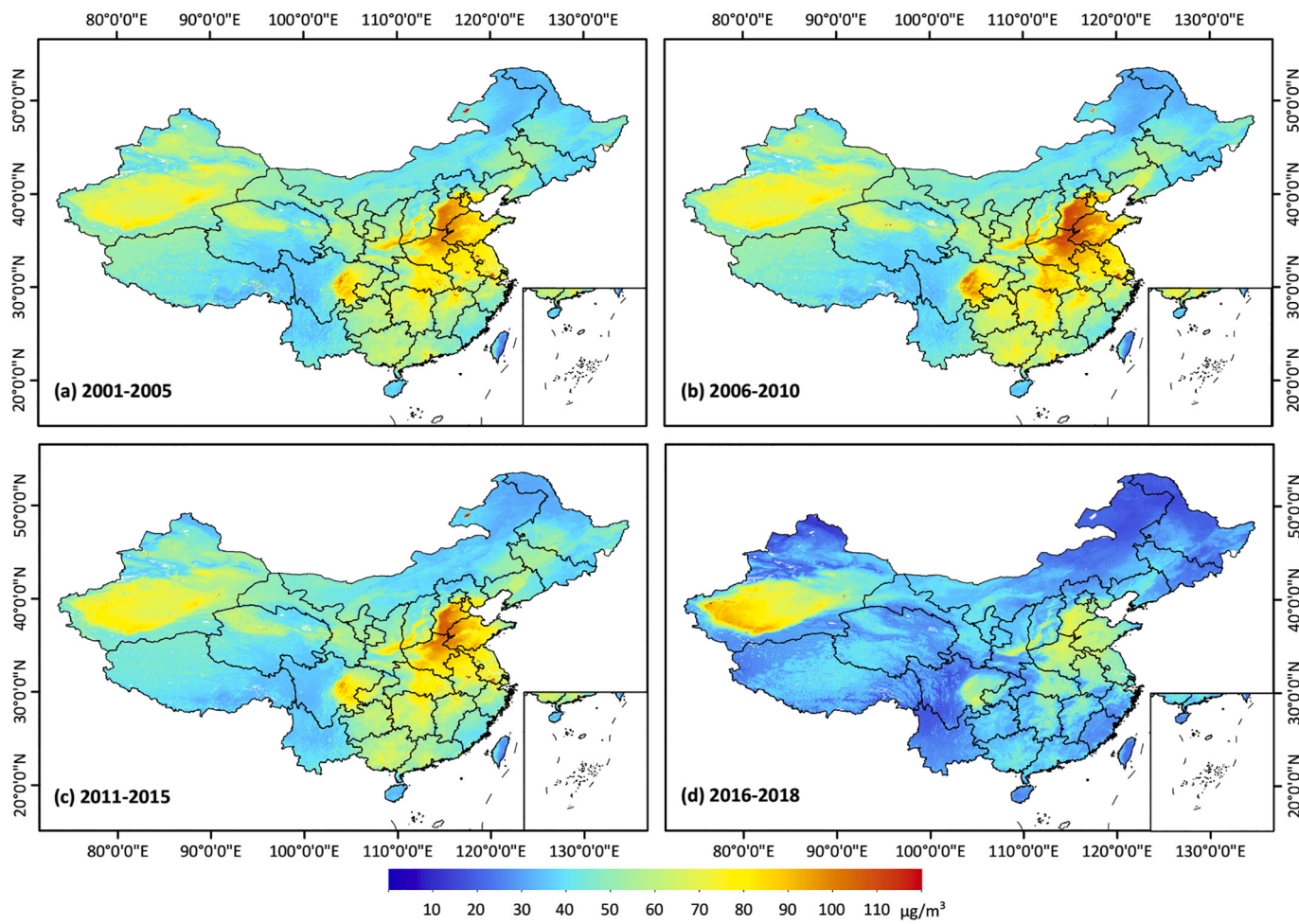


Fig. 14. MODIS-derived mean 1-km-resolution PM_{2.5} maps during the periods (a) 2001–2005, (b) 2006–2010, (c) 2011–2015, and (d) 2016–2018 in China.

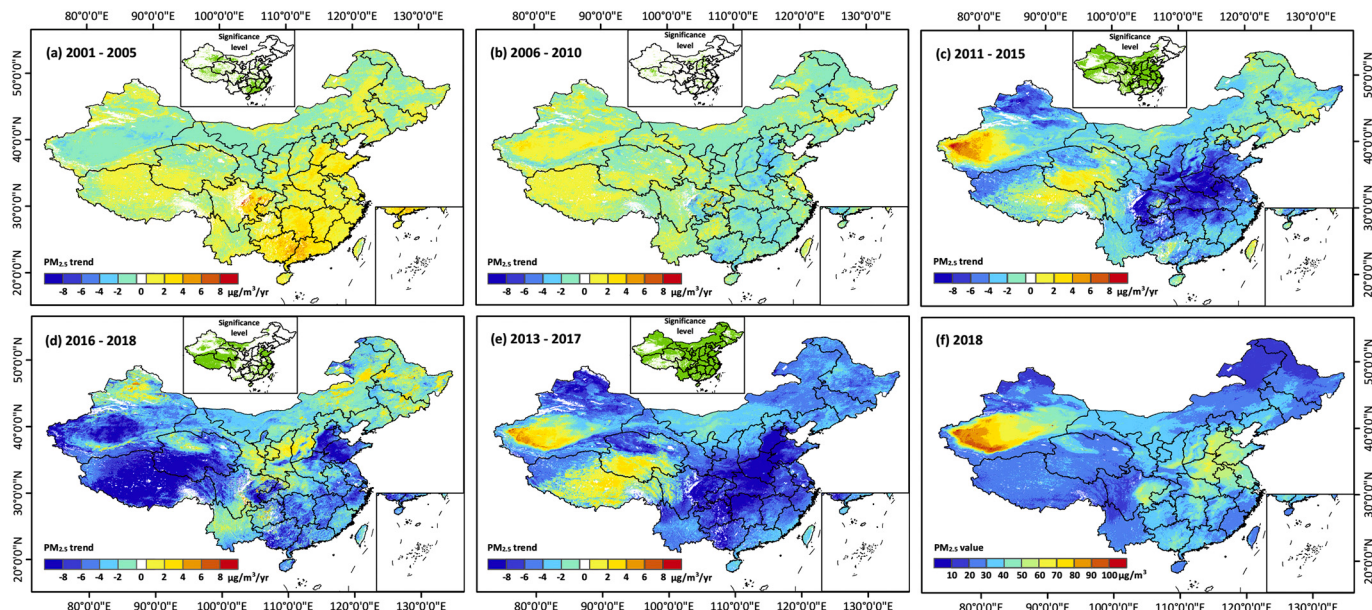


Fig. 15. Spatial distributions of PM_{2.5} trends ($\mu\text{g}/\text{m}^3/\text{yr}$) during the periods (a) 2001–2005, (b) 2006–2010, (c) 2011–2015, (d) 2016–2018, (e) 2013–2017, and (f) the annual mean PM_{2.5} map for 2018, where the green areas in the inset figures represent trends that are significant at the 95% ($p < 0.05$) confidence level. (For interpretation of the references to colour in this figure legend, the reader is referred to the web version of this article.)

Table 4

Statistics of annual PM_{2.5} trends ($\mu\text{g}/\text{m}^3/\text{yr}$) and their significance levels (p) across China and typical regions for different study periods.

Region	Period: 2001–2005		Period: 2006–2010		Period: 2011–2015		Period: 2016–2018	
	Trend	p	Trend	p	Trend	p	Trend	p
China	0.19	0.52	-0.29	0.24	-2.70	< 0.001	-4.26	< 0.001
ECHN	1.02	< 0.05	-0.44	0.26	-4.03	< 0.001	-3.07	< 0.001
BTH	1.13	0.12	-1.18	0.08	-3.72	< 0.01	-4.78	< 0.01
YRD	0.93	< 0.05	-0.05	0.92	-4.33	< 0.001	-4.05	< 0.01
PRD	1.36	< 0.05	-0.77	0.28	-2.60	< 0.01	-2.96	< 0.05
SCB	1.15	0.17	-0.30	0.67	-5.24	< 0.001	-2.80	< 0.05

BTH: Beijing-Tianjin-Hebei; ECHN: eastern China; PRD: Pearl River Delta; SCB: Sichuan Basin; YRD: Yangtze River Delta.

Table 5

Statistics of annual mean PM_{2.5} concentrations ($\mu\text{g}/\text{m}^3$), temporal trends ($\mu\text{g}/\text{m}^3/\text{yr}$), and relative change percentages (%) from 2013 to 2018 across China and local regions, where *** represent trends that are significant at the 99.9% ($p < 0.001$) confidence level.

Region	Annual mean PM _{2.5} concentrations			Trend (2013–2017)		Decreased by	
	2013	2017	2018	Satellite	Ground	2013–2017	2017–2018
China	53.5 ± 16.6	36.0 ± 14.2	32.6 ± 14.1	-4.13***	-5.22***	32.7%	9.4%
ECHN	60.5 ± 19.4	39.1 ± 11.5	34.6 ± 10.5	-6.11***	-5.32***	35.4%	11.5%
BTH	66.8 ± 27.6	45.1 ± 14.4	40.7 ± 11.8	-6.65***	-6.67***	32.5%	9.8%
YRD	67.2 ± 14.4	42.8 ± 8.4	38.1 ± 9.1	-6.51***	-6.09***	36.3%	11.0%
PRD	55.9 ± 7.9	38.3 ± 5.6	32.0 ± 4.4	-3.80***	-2.98***	31.5%	16.4%
SCB	72.3 ± 18.4	40.6 ± 11.7	38.4 ± 10.1	-8.00***	-6.61***	43.8%	5.4%
Beijing	59.5 ± 17.5	42.2 ± 9.6	37.9 ± 7.7	-5.84***	-5.43***	29.1%	10.2%

BTH: Beijing-Tianjin-Hebei; ECHN: eastern China; PRD: Pearl River Delta; SCB: Sichuan Basin; YRD: Yangtze River Delta.

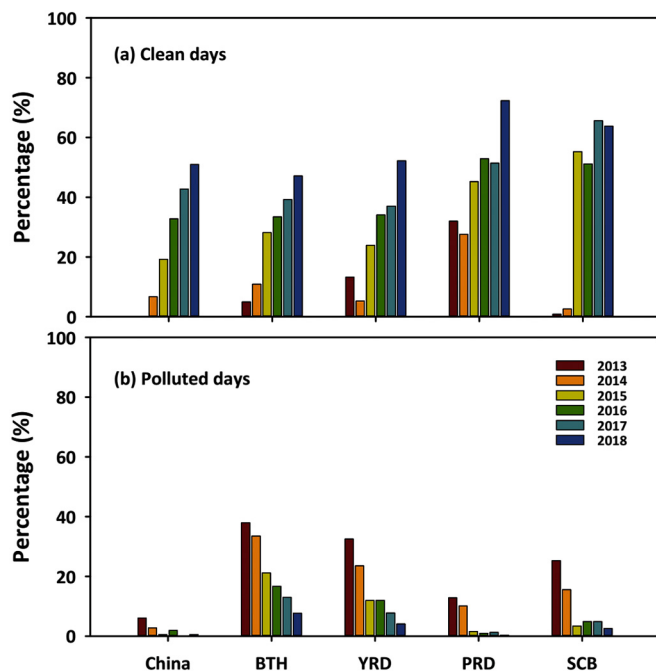


Fig. 16. Percentage variations of clear and polluted days when daily mean PM_{2.5} concentrations were (a) below 35 $\mu\text{g}/\text{m}^3$ and (b) exceeded 75 $\mu\text{g}/\text{m}^3$ from 2013 to 2018 across China and in four typical regions.

PRD), respectively, from 2013 to 2017. These results illustrate that China has reached the major goals set by the government regarding reducing PM_{2.5} pollution. Our satellite-based results are also close to the official evaluation results based on in situ observations (http://www.mee.gov.cn/gkml/stbjgw/stbgh/201806/t20180601_442262.htm). Air quality in Beijing had also improved significantly, with annual mean PM_{2.5} concentrations decreasing from $59.5 \pm 17.5 \mu\text{g}/\text{m}^3$ in 2013 to $42.2 \pm 9.6 \mu\text{g}/\text{m}^3$ in 2017, which also exceeded the set goal (i.e., PM_{2.5} $\approx 60 \mu\text{g}/\text{m}^3$). Moreover, PM_{2.5} pollution was overall reduced in $\sim 98\%$ of

prefecture-level cities, with decreases of $>20\%$ at more than 89% of these cities (Fig. S9). Upgraded industrial structures and enhanced emission controls on primary particles and SO₂ from industrial enterprises, including coal consumption, were responsible for this improvement in air quality (Li et al., 2019b; Zhang et al., 2019a).

By the end of the first year of the Blue-Sky Defense (2018), except for Xinjiang province and the North China Plain, most areas had overall low PM_{2.5} concentrations across mainland China (average = $32.6 \pm 14.1 \mu\text{g}/\text{m}^3$), especially in summer ($\sim 25.2 \pm 12.4 \mu\text{g}/\text{m}^3$) and winter ($\sim 41.4 \pm 15.6 \mu\text{g}/\text{m}^3$). PM_{2.5} concentrations had declined continuously by 10–16% in three key regions (Table 5), and $\sim 70\%$ of China's expanse and 57% of prefecture-level cities (Fig. S6) had PM_{2.5} concentrations that fell below the acceptable national air quality standard. The number of clean days (PM_{2.5} $< 35 \mu\text{g}/\text{m}^3$) had also continuously increased, while the number of polluted days (PM_{2.5} $> 75 \mu\text{g}/\text{m}^3$) had continuously decreased from 2013 to 2018 across China and in some regions, in particular, the PRD region. That region had the greatest number of clear days ($\sim 72\%$) and almost no high-pollution days ($< 1\%$) in 2018 (Fig. 16), indicating that China's air quality had improved significantly. However, some regions still experienced high pollution levels, e.g., the BTH and YRD regions, requiring further measures to be taken in the future.

4. Summary and conclusions

Here, a newly developed Space-Time Extra-Trees (STET) model was employed to establish robust PM_{2.5}-AOD relationships for mainland China by incorporating spatiotemporal information and information about surface conditions and human activities. Results show that the model is more accurate in estimating current PM_{2.5} concentrations (e.g., cross-validation R² = 0.86–0.90) and in predicting historical PM_{2.5} concentrations (e.g., R² = 0.80–0.82) across China than most models developed in previous studies. This model, for the first time, helped reconstruct a high-resolution (1 km) and high-quality PM_{2.5} dataset for mainland China (i.e., the ChinaHighPM_{2.5} product) from 2000 to 2018. The 1 km spatial resolution of the product allows for the analysis of PM_{2.5} exposure and pollution variations from national, regional, to urban scales across China.

Results show that most of mainland China experienced high PM_{2.5}

exposure risks, especially in winter. However, PM_{2.5} pollution has greatly changed during the last two decades due to the implementation of different government policies. PM_{2.5} concentrations were significantly increasing before 2008 due to rapid economic development and remained relatively stable until 2012. Since 2013, PM_{2.5} concentrations have decreased, benefiting from large-scale air pollution prevention and controls in China. This ChinaHighPM_{2.5} dataset is potentially useful for understanding long-term PM_{2.5} burdens and variations at medium to small scales.

Data availability

The ChinaHighPM_{2.5} dataset is open access and freely available to all users from <https://weijing-rs.github.io/product.html>.

Declaration of Competing Interest

None.

Acknowledgments

This work was supported by the National Key R&D Program of China (2017YFC1501702), the National Important Project of the Ministry of Science and Technology in China (2017YFC1501404), and the National Natural Science Foundation of China (41705125). The first author was supported by the Shanghai Tongji Gao Tingyao Environmental Science & Technology Development Foundation. We would like to thank Dr. Qiang Zhang at Tsinghua University and Dr. Zongwei Ma at Nanjing University for providing MEIC emission and surface PM_{2.5} data for China.

Appendix A. Supplementary data

Supplementary data to this article can be found online at <https://doi.org/10.1016/j.rse.2020.112136>.

References

- Beelen, R., Raaschou-Nielsen, O., Stafoggia, M., Andersen, Z., Weinmayr, G., Hoffmann, B., et al., 2014. Effects of long-term exposure to air pollution on natural-cause mortality: an analysis of 22 European cohorts within the multicentre ESCAPE project. *Lancet* 383 (9919), 785–795. [https://doi.org/10.1016/S0140-6736\(13\)62158-3](https://doi.org/10.1016/S0140-6736(13)62158-3).
- Brauer, M., Anann, M., Burnett, R., Cohen, A., Dentener, F., Ezzati, M., Thurston, G., 2012. Exposure assessment for estimation of the global burden of disease attributable to outdoor air pollution. *Environ. Sci. Technol.* 46 (2), 652–660.
- Breiman, L., 2001. Random forests. *Mach. Learn.* 45, 5–32.
- Chen, G., Li, S., Knibbs, L., Hamm, N., Cao, W., Li, T., Guo, J., Ren, H., Abramson, M., Guo, Y., 2018. A machine learning method to estimate PM_{2.5} concentrations across China with remote sensing, meteorological and land use information. *Sci. Total Environ.* 636, 52–60.
- Chen, Z., Zhang, T., Zhang, R., Zhu, Z., Yang, J., Chen, P., Ou, C., Guo, Y., 2019. Extreme gradient boosting model to estimate PM_{2.5} concentrations with missing-filled satellite data in China. *Atmos. Environ.* 202, 180–189.
- Cohen, A., Brauer, M., Burnett, R., Anderson, H., Frostad, J., Estep, K., 2017. Estimates and 25-year trends of the global burden of disease attributable to ambient air pollution: an analysis of data from the global burden of diseases study 2015. *Lancet* 289 (10082), 1907–1918. [https://doi.org/10.1016/S0140-6736\(17\)30505-6](https://doi.org/10.1016/S0140-6736(17)30505-6).
- Dee, D., Uppala, S., Simmons, A., Berrisford, P., Poli, P., Kobayashi, S., Vitart, F., 2011. The ERA-interim reanalysis: configuration and performance of the data assimilation system. *J. Meteorol. Soc. Jpn.* 137 (656), 553–597.
- Dobson, J., Bright, E., Coleman, P., Durfee, R., Worley, B.A., 2000. Global population database for estimating populations at risk. *Photogramm. Eng. Remote. Sens.* 66(7).
- Du, X., Mendelsohn, R., 2011. Estimating the value of the reduction in air pollution during the Beijing Olympics. *Environ. Dev. Econ.* 16 (6), 735–749.
- Geurts, P., Ernst, D., Wehenkel, L., 2006. Extremely randomized trees. *Machine Learn.* 63 (1), 3–42.
- Guo, J., Zhang, X., Che, H., Gong, S., An, X., Cao, C., et al., 2009. Correlation between PM concentrations and aerosol optical depth in eastern China. *Atmos. Environ.* 43 (37), 5876–5886.
- Guo, J., Miao, Y., Zhang, Y., Liu, H., Li, Z., Zhang, W., He, J., Lou, M., Yan, Y., Bian, L., Zhai, P., 2016. The climatology of planetary boundary layer height in China derived from radiosonde and reanalysis data. *Atmos. Chem. Phys.* 16, 13,309–13,319.
- Hammer, M., van Donkelaar, A., Li, C., Lyapustin, A., Sayer, A., Hsu, N., Levy, R., Garay, M., Kalashnikova, O., Kahn, R., Brauer, M., Apte, Joshua, Henze, D., Zhang, L., Zhang, Q., Ford, B., Pierce, J., Martin, R., 2020. Global Estimates and Long-Term Trends of Fine Particulate Matter Concentrations (1998–2018). *Environ. Sci. Technol.* 54 (13), 7879–7890.
- He, Q., Zhang, M., Huang, B., Tong, X., 2017. MODIS 3 km and 10 km aerosol optical depth for China: evaluation and comparison. *Atmos. Environ.* 153, 150–162.
- Hong, C., Zhang, Q., Zhang, Y., Davis, S., Tong, D., Zheng, Y., Liu, Z., Guan, D., He, K., Schellnhuber, H., 2019. Impacts of climate change on future air quality and human health in China. *Proc. Natl. Acad. Sci.* 116 (35), 201812881. <https://doi.org/10.1073/pnas.1812881116>.
- Jiang, R., Tang, W., Wu, X., Fu, W., 2009. A random forest approach to the detection of epistatic interactions in case-control studies. *BMC Bioinformatics* 10, 135.
- Li, Z., Guo, J., Ding, A., Liao, H., Liu, J., Sun, Y., Wang, T., Xue, H., Zhang, H., Zhu, B., 2017a. Aerosol and boundary-layer interactions and impact on air quality. *Natl. Sci. Rev.* 4 (6), 810–833. <https://doi.org/10.1093/nsr/nwx117>.
- Li, T., Shen, H., Yuan, Q., Zhang, X., Zhang, L., 2017b. Estimating ground-level PM_{2.5} by fusing satellite and station observations: a geo-intelligent deep learning approach. *Geophys. Res. Lett.* 44 (23), 11,985–11,993.
- Li, M., Zhang, Q., Kurokawa, J., Woo, J., He, K., Lu, Z., Ohara, T., Song, Y., Streets, D., Carmichael, G., Cheng, Y., Hong, C., Huo, H., Jiang, X., Kang, S., Liu, F., Su, H., Zheng, B., 2017c. MIX: a mosaic Asian anthropogenic emission inventory under the international collaboration framework of the MICS-Asia and HTAP. *Atmos. Chem. Phys.* 17, 935–963.
- Li, K., Jacob, D.J., Liao, H., Zhu, J., Shah, V., Shen, L., Bates, K., Zhang, Q., Zhai, S., 2019a. A two-pollutant strategy for improving ozone and particulate matter air quality in China. *Nat. Geosci.* 12(11). <https://doi.org/10.1038/s41561-019-0464-x>.
- Li, C., Li, J., Xu, H., Li, Z., Xia, X., Che, H., 2019b. Evaluating VIIRS EPS aerosol optical depth in China: an intercomparison against ground-based measurements and MODIS. *J. Quant. Spectrosc. Radiat. Transf.* 224, 368–377.
- Li, Z., Wang, Y., Guo, J., Cribb, M.C., Dong, X., Fan, J., et al., 2019c. East Asian Study of Tropospheric aerosols and their impact on regional clouds, precipitation, and climate (EAST-AIR_{CPC}). *J. Geophys. Res.-Atmos.* 124. <https://doi.org/10.1029/2019JD030758>.
- Lin, C., Liu, G., Lau, A., Li, Y., Li, C., Fung, J., Lao, X., 2018. High-resolution satellite remote sensing of provincial PM_{2.5} trends in China from 2001 to 2015. *Atmos. Environ.* 180, 110–116.
- Liu, C., Chen, R., Sera, F., Vicedo-Cabrara, A.M., Guo, Y., et al., 2019a. Ambient particulate air pollution and daily mortality in 652 cities. *N. Engl. J. Med.* 381, 705–715.
- Liu, N., Zou, B., Feng, H., Wang, W., Tang, Y., Liang, Y., 2019b. Evaluation and comparison of multi-angle implementation of the atmospheric correction algorithm, dark target, and deep blue aerosol products over China. *Atmos. Chem. Phys.* 19, 8243–8268.
- Lyapustin, A., Wang, Y., Korkin, S., Huang, D., 2018. MODIS collection 6 MAIAC algorithm. *Atmos. Measure Tech.* 11, 5741–5765.
- Ma, Z., Hu, X., Huang, L., Bi, J., Liu, Y., 2014. Estimating ground-level PM_{2.5} in China using satellite remote sensing. *Environ. Sci. Technol.* 48 (13), 7436–7444.
- Ma, Z., Hu, X., Sayer, A., Levy, R., Zhang, Q., Xue, Y., Tong, S., Bi, J., Huang, L., Liu, Y., 2016. Satellite-based spatiotemporal trends in PM_{2.5} concentrations: China, 2004–2013. *Environ. Health Perspect.* 124, 184–192.
- Misra, A., Tripathi, S., Kaul, D., Welton, E., 2012. Study of MPLNET-derived aerosol climatology over Kanpur, India, and validation of CALIPSO level 2 version 3 backscatter and extinction products. *J. Atmos. Ocean. Technol.* 29 (9), 1285–1294.
- Pappalardo, G., Wandinger, U., Mona, L., Hiebsch, A., Mattis, I., Amodeo, A., Ansman, A., Seifert, P., Linné, H., Apituley, A., Arboledas, L., 2010. EARLINET correlative measurements for CALIPSO: first intercomparison results. *J. Geophys. Res.-Atmos.* 115 (D4) <https://doi.org/10.1029/2009JD012147>.
- Rodriguez, J., Perez, A., Lozano, J., 2010. Sensitivity analysis of k-fold cross validation in prediction error estimation. *IEEE Trans. Pattern Anal. Mach. Intell.* 32 (3), 569–575.
- Shen, J., Tang, A., Liu, X., Kopsch-Xhema, J., Fangmeier, A., Goulding, K., 2011. Impacts of pollution controls on air quality in Beijing during the 2008 Olympic Games. *J. Environ. Qual.* 40 (1), 37–45.
- Song, Y., Huang, B., He, Q., Chen, B., Wei, J., Mahmood, R., 2019. Dynamic assessment of PM_{2.5} exposure and health risk using remote sensing and geo-spatial big data. *Environ. Pollut.* 253, 288–296.
- Su, T., Laszlo, I., Li, Z., Wei, J., Kalluri, S., 2020. Refining aerosol optical depth retrievals over land by constructing the relationship of spectral surface reflectances through deep learning: Application to Himawari-8. *Remote Sens. Environ.* 251, 112093. <https://doi.org/10.1016/j.rse.2020.112093>.
- Su, T., Li, Z., Kahn, R., 2018. Relationships between the planetary boundary layer height and surface pollutants derived from lidar observations over China: regional pattern and influencing factors. *Atmos. Chem. Phys.* 18 (21), 15,921–15,935.
- Su, T., Li, Z., Kahn, R., 2020. A new method to retrieve the diurnal variability of planetary boundary layer height from lidar under different thermodynamic stability conditions. *Remote Sens. Environ.* 237, 111519.
- Sun, L., Wei, J., Duan, D., Guo, Y., Yang, D., Jia, C., Mi, X., 2016. Impact of land-use and land-cover change on urban air quality in representative cities of China. *J. Atmos. Sol. Terr. Phys.* 142, 43–54.
- Tao, M., Wang, J., Li, R., Wang, L., Wang, Z., Tao, J., Che, H., Chen, L., 2019. Performance of MODIS high-resolution MAIAC aerosol algorithm in China: characterization and limitation. *Atmos. Environ.* 213, 159–169.
- Toth, T., Zhang, J., Campbell, J., Hyer, E., Reid, J., Shi, Y., Westphal, D., 2014. Impact of data quality and surface-to-column representativeness on the PM_{2.5}/satellite AOD relationship for the contiguous United States. *Atmos. Chem. Phys.* 14, 6049–6062. <https://doi.org/10.5194/acp-14-6049-2014>.

- Toth, T., Zhang, J., Reid, J., Vaughan, M., 2019. A bulk-mass-modeling-based method for retrieving particulate matter pollution using CALIOP observations. *Atmos. Measure Tech.* 12, 1739–1754. <https://doi.org/10.5194/amt-12-1739-2019>.
- van Donkelaar, A., Martin, R., Park, R., 2006. Estimating ground-level PM_{2.5} using aerosol optical depth determined from satellite remote sensing. *J. Geophys. Res.-Atmos.* 111, D21201 <https://doi.org/10.1029/2005JD006996>.
- Wang, W., Mao, F., Pan, Z., Gong, W., Yoshida, M., Zou, B., Ma, H., 2019. Evaluating aerosol optical depth from Himawari-8 with Sun photometer network. *J. Geophys. Res.-Atmos.* 124 <https://doi.org/10.1029/2018JD028599>.
- Wei, J., Sun, L., Huang, B., Bilal, M., Zhang, Z., Wang, L., 2018a. Verification, improvement and application of aerosol optical depths in China. Part 1: inter-comparison of NPP-VIIRS and aqua-MODIS. *Atmos. Environ.* 175, 221–233.
- Wei, J., Sun, L., Peng, Y., Wang, L., Zhang, Z., Bilal, M., Ma, Y., 2018b. An improved high-spatial-resolution aerosol retrieval algorithm for MODIS images over land. *J. Geophys. Res.-Atmos.* 123, 12,291–12,307.
- Wei, J., Li, Z., Guo, J., Sun, L., Huang, W., Xue, W., Fan, T., Cribb, M., 2019b. Satellite-derived 1 km-resolution PM₁ concentrations from 2014 to 2018 across China. *Environ. Sci. Technol.* 53 (22), 13,265–13,274. <https://doi.org/10.1021/acs.est.9b03258>.
- Wei, J., Li, Z., Peng, Y., Sun, L., 2019c. MODIS collection 6.1 aerosol optical depth products over land and ocean: validation and comparison. *Atmos. Environ.* 201, 428–440.
- Wei, J., Li, Z., Peng, Y., Sun, L., Yan, X., 2019d. A regionally robust high-spatial-resolution aerosol retrieval algorithm for MODIS images over eastern China. *IEEE Transac. Geosci. Remote Sens.* 57 (7), 4748–4757.
- Wei, J., Peng, Y., Mahmood, R., Sun, L., Guo, J., 2019e. Intercomparison in spatial distributions and temporal trends derived from multi-source satellite aerosol products. *Atmos. Chem. Phys.* 19, 7183–7207.
- Wei, J., Huang, W., Li, Z., Xue, W., Peng, Y., Sun, L., Cribb, M., 2019a. Estimating 1 km-resolution PM_{2.5} concentrations across China using the space-time random forest approach. *Remote Sens. Environ.* 231, 111221. <https://doi.org/10.1016/j.rse.2019.111221>.
- Wei, J., Li, Z., Cribb, M., Huang, W., Xue, W., Sun, L., Guo, J., Peng, Y., Li, J., Lyapustin, A., Liu, L., Wu, H., Song, Y., 2020. Improved 1 km resolution PM_{2.5} estimates across China using enhanced space-time extremely randomized trees. *Atmos. Chem. Phys.* 20 (6), 3273–3289.
- Wu, Y., Cordero, L., Gross, B., Moshary, F., Ahmed, S., 2014. Assessment of CALIPSO attenuated backscatter and aerosol retrievals with a combined ground-based multi-wavelength lidar and sunphotometer measurement. *Atmos. Environ.* 84, 44–53.
- Xin, J., Wang, Y., Pan, Y., Ji, D., Liu, Z., et al., 2015. The campaign on atmospheric aerosol research network of China. *Bull. Am. Meteorol. Soc.* 96 (7), 1137–1155. <https://doi.org/10.1175/BAMS-D-14-00039.1>.
- Xue, T., Zheng, Y., Tong, D., Zheng, B., Li, X., Zhu, T., Zhang, Q., 2019. Spatiotemporal continuous estimates of PM_{2.5} concentrations in China, 2000–2016: a machine learning method with inputs from satellites, chemical transport model, and ground observations. *Environ. Int.* 201, 345–357, 123.
- Yan, X., Shi, W., Li, Z., Li, Z., Luo, N., Zhao, W., Wang, H., Yu, X., 2017. Satellite-based PM_{2.5} estimation using fine-mode aerosol optical depth thickness over China. *Atmos. Environ.* 170, 290–302. <https://doi.org/10.1016/j.atmosenv.2017.09.023>.
- Yana, J., Henrik, A., Shiqiu, Z., 2016. Air pollution control policies in China: a retrospective and prospects. *Int. J. Environ. Res. Public Health* 13 (13), 1219. <https://doi.org/10.3390/ijerph13121219>.
- Yao, F., Wu, J., Li, W., Peng, J., 2019. A spatially structured adaptive two-stage model for retrieving ground-level PM_{2.5} concentrations from VIIRS AOD in China. *ISPRS J. Photogramm. Remote Sens.* 151, 263–276.
- Yu, W., Liu, Y., Ma, Z., Bi, J., 2017. Improving satellite-based PM_{2.5} estimates in China using Gaussian processes modeling in a Bayesian hierarchical setting. *Sci. Rep.* 7, 7048. <https://doi.org/10.1038/s41598-017-07478-0>.
- Zhang, Y., Li, Z., 2015. Remote sensing of atmospheric fine particulate matter (PM_{2.5}) mass concentration near the ground from satellite observation. *Remote Sens. Environ.* 160, 252–262.
- Zhang, Q., Streets, D., He, K., Klimont, Z., 2007. Major components of China's anthropogenic primary particulate emissions. *Environ. Res. Lett.* 2 (No. 045027).
- Zhang, Q., Zheng, Y., Tong, D., Shao, M., Wang, S., et al., 2019a. Drivers of improved PM_{2.5} air quality in China from 2013 to 2017. *Proc. Natl. Acad. Sci. U. S. A.* <https://doi.org/10.1073/pnas.1907956116>.
- Zhang, Z., Wu, W., Fan, M., Tao, M., Wei, J., Jin, J., Tan, Y., Wang, Q., 2019b. Validation of Himawari-8 aerosol optical depth retrievals over China. *Atmos. Environ.* 199, 32–44.
- Zhang, T., Zang, L., Wan, Y., Wang, W., Zhang, Y., 2019c. Ground-level PM_{2.5} estimation over urban agglomerations in China with high spatiotemporal resolution based on Himawari-8. *Sci. Total Environ.* 676, 535–544.
- Zhou, C., Wang, K., 2016. Evaluation of surface fluxes in ERA-interim using flux tower data. *J. Clim.* 29, 1573–1582.
- Zhou, C., He, Y., Wang, K., 2018. On the suitability of current atmospheric reanalyses for regional warming studies over China. *Atmos. Chem. Phys.* 18, 8113–8136.